COMPONENT PART NOTICE

THIS PAPER IS A COMPONENT PART OF THE FOLLOWING COMPILATION REPORT:

TITLE: Microwave Antennas for Avionics. Lecture Series of the ~~Panel~~ Avionics Panel and the Consultant and Exchange Programme Held in Rome, Italy on 7-8 May 1987; Guenzburg, Germany on 11-12 May 1987 and Ankara, Turkey on 14-15 May 1987.

TO ORDER THE COMPLETE COMPILATION REPORT, USE AD-A185 152.

THE COMPONENT PART IS PROVIDED HERE TO ALLOW USERS ACCESS TO INDIVIDUALLY AUTHORED SECTIONS OF PROCEEDING, ANNALS, SYMPOSIA, ETC. HOWEVER, THE COMPONENT SHOULD BE CONSIDERED WITHIN THE CONTEXT OF THE OVERALL COMPILATION REPORT AND NOT AS A STAND-ALONE TECHNICAL REPORT.

THE FOLLOWING COMPONENT PART NUMBERS COMPRISE THE COMPILATION REPORT:

AD#: P005 663 AD#: P005 670

AD#: AD#:

AD#: AD#:

Accession For	
NTIS GRA&I	☒
DTIC TAB	☐
Unannounced	☐
Justification	
By	
Distribution/	
Availability Codes	
Dist	Avail and/or Special
A-1	

SPACECRAFT MULTI-BEAM AND CONTOURED-BEAM ANTENNAS

by
P. Balling
TICRA
Kronprinsensgede 13
DK-1114 Copanhagen K
Danmark

SUMMARY

High-gain spacecreft antennas with multiple beams and contoured beams ara kay components in satellite communicetions and direct broedcast systems. This is reflected on the latest genaration of communications setellites, where the entenna subsystem is the largest subeystem with its weight of mora than 300 kg. The entannas achieva e lerge communications capacity through multipla frequency re-uses and may be racon-figured to serve diffarent covarage araas.

The peper overviews the currant multi-beem and contoured-baam entanna technology. Different impleman-tations, reflector or lens with faad erray or direct redieting array, ere considerad. Tha emphesis is placad upon systems with offeet paraboloidal reflectors. The limitetione of the offset reflector with respect to beam scanning end crose polarization ere reviewed. Computar-eided dasign procedures end dasign examplas ara presented.

1. INTRODUCTION

The antenne syetems cerried on boerd spacecreft have over the lest 25 yeers undergone e rapid evolu-tion which parellels thet of the spececraft themselves. In fact, the spacecreft system requirements have bean end continue to be a main driving force behind tha rejuvenetion of entanna thaory and technology which previously ware considerad to be mature disciplines. This evolution hae baan eupported by the eimulteneous edvent of ebundant computetionel fecilities.

Early spacecreft were emall, spin-stabilized setellites in low orbite. Tha antanne systeme wara simple, oftan with a low power in a nerrow frequency band, typically in the VHF band. Currant spacecraft hava become lerge end highly specielised end often carry saverel antenna eysteme which era teilored to the role of tha spacecreft. Most communicetions spececraft ere plecad elong the geoetetionary arc some 36,000 km above the surfece of the Eerth. The multi-beam and the contourad-baam antennes reviewed in thie papar ara examplee of perticularly complex antenne syetems which significently increase the cepacity end flexi-bility of theee aetellite eystams. By international agraement certein frequancy bands heva bean allocatad for the different setellites servicae end rules heva been sat to minimiza the interferenca with othar satellite eyetems end with sarth-beeed systems [1]. Typically, the uplink signale from tha Eerth to the satellite end tha downlink signels back to the Eerth use different bande. Some of the most importent fre-quency-band allocetions for tha fixad satellite eervices (communicetions eetellitas) era indiceted in Teble 1. Tha frequency allocations differ elightly for three CCIR regions of the world and various rastrictions may epply so that the full bands cannot be used. Other bande era alloceted for communication with mobile stations and for direct broadcast. Additionel bande ere alloceted at highar frequencies. Initially, the lower bands hava been the most popular as the technology has been better daveloped.

	Uplink	Downlink
C-band	5.925- 7.250 GHs	3.400- 4.200 and 4.500- 4.800 GHs
Ku-band	12.500-13.250 and 14.000-14.800 GHs	10.700-11.700 GHs
Ka-band	27.500-31.000 GHs	18.100-21.200 GHs

Table 1. CCIR allocations for tha fixad-satallite servica

1.1 Multi-Beam Antennas

Tha finita frequency spactrum availabla and the finite number of slots along tha geostationary arc for satellitas operating in the same frequency bend ara best utilisad by a multi-baam antenna which illu-minates the covaraga area by a eumber of element beams. A hexagonal baam lattice is the most efficiant for contiguous area covarage. If the antenna radiates N beams and the available frequancy spectrum is divided into K bands or channels so that adjacent baams usa differant bands, the frequancy spectrum can be re-used M=N/K times. Figure 1 shows differant beam topologias whera the number in asch call or beam foot print gives tha channel number. The more channels the frequency band is divided into, the larger tha spacing will be between the calls where the same frequency is re-used and the better the isolation will be batween thesa beams. However, the number of times the frequency is re-usad will be lass. In practical systems, adjacent or overlapping beams may use orthogonal polarisations to improve the isolation or increase the number of frequenoy re-usea.

As an additional advantage of dividing the ooverage area into smaller celle, the spacecraft antenna gain is drastically increased. If all the power radiated by tha satellite were uniformly distributed over ±8.7° field-of-view subtended by tha Earth, tho ultimataly achievable gain would be 22.4 dBi. This would require an infinitely large, losslees antenna. In practice leee than 17 dBi is obtained towards the edge of the Earth using e horn antenna. With a multi-beam antanna, the upper limit on the achievable gain would ba eet by eise of the element-beam foot print or by the acceptable sise and complexity of the antenna system and the accuracy with which tha aetenna can be kept pointed towards the coverage area. This shift from the early low-gain over medium-gain spacecraft antennas, which required huge earth-station antennas, to high-gain spacecraft antennas with small beam foot prints has in conjunction with improvements in satellite power and low-noise receivers lead to the introduction of comparatively cheap, small earth-station antennas. More aspects of multi-beam antennas are discussed in [2-4].

The simple beam topologies of Figure 1 carry some disadvantages. In real life, the communications requirements are not uniformly distributed over the field-of-view and a multi-beam antenna system with many beams requires many transponders and a large switch matrix to provide the inter-connectivity between the uplink and the downlink beams. Also, it has not yet been practical without the use of several antennas or excessive antenna losses to radiate element beams with the crossover levels down from the beam peak in the order of 3-4 dB needed for a contiguous coverage. These problems have lead to the concept of contoured-beam antennas where several of the element beams are combined in a cluster or a composite beam.

1.2 Contoured-Beam Antennas

A contoured-beam antenna provides one or more beams with foot prints on the Earth tailored to specific geographical areas. Sometimes these antennas are referred to as multi-beam antennas or shaped-beam antennas. The beam-contouring conserves the satellite power and reduces the interference both with adjacent frequency re-use coverage areas of the same satellite system and with other systems. Figure 2 illustrates the most common hardware used to generate a contoured beam: a feed array which illuminates an offset paraboloidal reflector. Each feed element, usually a small horn, generates a scanned pencil beam which is termed an element beam or a component beam. The foot prints of these element beams on the Earth are indicated by small circles on Figure 2. A contoured beam which provides service to coverage area A is obtained by adding the element beams radiated towards the coverage area with appropriate (complex) weight factors. These weights or feed excitations are generated by a beam-forming network (BFN) which often is a power divider tree with phase shifts provided by line length differences at the feed ports.

The feed array and in particular the BFN are the most critical parts of a contoured-beam reflector antenna as they must realize the desired feed excitations with acceptable amplitude and phase tolerances and low VSWRs at both the feed ports and the beam port over the operating frequency bandwidth. The antenna system is required to operate in a hostile space environment with temperature excursions in the order of -60 to 60 °C or more over the 7 to 10 year satellite lifetime. The BFNs of most current contoured-beam antennas consist of fixed power dividers and phase shifters. These BFNs are usually implemented in TEM-line in the 6/4 GHz bands and in waveguide in the 14/11 and 30/20 GHz bands. Waveguide BFNs have lower insertion loss, but are heavier and more bulky than TEM-line BFNs. The stringent matching requirements have lead to the almost exclusive use of hybrid couplers rather than simple 3-port TEEs or E-plane couplers in the power divider tree.

Advanced antenna systems include on international communications satellites switches to provide slowly reconfigurable beams to allow a satellite to operate from different locations along the geostationary arc and to accommodate traffic changes and on DSCS III fully reconfigurable BFNs with variable ferrite power dividers. Future systems are likely to include more variable power dividers and variable phase shifters in ferrite or solid-state technology. This will allow both a high degree of beam flexibility and the fast reconfigurability required for hopping and scanning beams with TDMA. Ultimately, BFNs are expected to include many active components to compensate for losses. This will provide very compact and flexible BFNs.

If the antenna system only is required to generate a single fixed contoured beam, a shaped reflector illuminated by a single feed is an attractive solution with respect to both performance and cost mainly because no BFN is required. This concept is reviewed in Section 5.

1.3 Choice of Reflector, Lens or Array?

The use of a focusing device such a reflector or a lens provides a one-to-one relation between the element beams and the feed horns. This relationship does not exist in the case of an array, where each array element contributes to all element beams, and an array with several independent beams operating at the same frequency and polarization would suffer from significant losses unless a Butler-matrix type BFN is used with orthogonal array illuminations for the different beams. In the cases of multi-beam antennas where each beam can be generated by a single feed and of contoured-beams antennas where only a few element beams are used to generate the contoured beam, the BFN is much simpler for a reflector and a lens. As a result, array antennas have found only little use as spacecraft multi-beam and contoured-beam antennas. Nevertheless, we will consider contoured-beam array antennas further in Section 7. A review of multi-beam arrays is given in [5].

The choice between reflector and lens is more difficult. In the past, most systems have used reflectors due to their low weight and cost, excellent bandwidth and polarization properties and the fact that they can be analysed very accurately with the existing RF analysis methods. A main disadvantage of the reflector is the need to use an offset-fed reflector geometry to avoid blockage by the large feed array, BFN and support structure. The offset-fed reflector has significantly worse scan and cross-polarization performance and occupies a larger volume on the spacecraft than a similar center-fed reflector.

The lens is a focusing device with axial symmetry but without blockage. As furthermore the remaining dominant scan aberration, coma, may be removed by choosing the inner lens surface to be a sphere so that the Abbé sine condition is fulfilled, lens antennas have considerable attraction for multi-beam applications [6]. Dielectric lenses are far too heavy for use at microwave frequencies on a spacecraft, and new low-weight but also more complicated lenses such as the zoned waveguide lens and the printed-circuit bootlace or TEM-line lens outlined in Figure 3 have been devised. These lenses may be attractive in systems with somewhat less than 100 element beams where the number of waveguide or printed-circuit elements can be kept reasonably small. The DSCS III spacecraft in fact flies three multi-beam zoned waveguide lens antennas operating at about 8 GHz [4]. The bandwidth of a zoned waveguide lens is not competible with thoss steted in Tabls 1. The more broadbanded TEM-line lene hes been invsstigatsd for use at C band [7]. However, ite weight was considersd to ba so largs that the receivs and ths transmit function would have to be combined in one entenne. The matching problem et the inner lene surfece could not be solved ovsr the combined frequency band and led to degradations of the element beams nsar tha axie. Becaues of their complexity and the still unsolved problems, lens entennas ere not considered further in this paper. It is expactsd that lens antennae will prove to be more useful at millimetsr and submillimeter wevelsngths.

Solid raflectors manufacturad from carbon-fiber re-enforcsd plastic (CFRP) heve become very populer dus to their low wsight and excellent thermal behavior. Surfacs accuraciee in the order of 1/100 wavelength RMS are requirsd to ensure low sidelobes. Solid offset reflectors providc excellent cross-polarization performance when ussd with circular polarization. Howsver, many domestic systems use linser polerizetion. This has led to the devslcpment of griddsd and duel gridded rsflectore to reduce the cross polerization introduced by the offsst configuration.

2. FUNDAMENTALS OF CONTOURED-BEAM REFLECTOR ANTENNAS

2.1. Basic Definitione

Contoured-beam reflsctor antsnna eyetems hevs e unique sst of performance parametera. Most other entenna systems, including eerth stetion entennae, optimize the on-axie gain subject to certain eidelobe constreints oftan definsd by en envelope. The driving eystem parameters are EIRP and G/T with sidelobe constraints edded to minimize interference. Cross-polarization requirements often only apply near the beam axis. Whsn en entenne is requirsd to ssrve an area rather than just e single direction, the minimum coverage area gain and not the peak gain becomee the eignificant parameter. Hence, tha etandard definition of antenna efficiency doee not apply to contoured-beam antennas. Tha efficiency η of a contoured beam entenne is defined as the ratio of ths minimum coveregs erea gein MCAG to the gain G_{un} of e lossleae entenne which distributes all the radiated power uniformly ecrose the specifisd coveraga arae Ω (in stsredians), i.e.,

$$\eta = MCAG/G_{un} \tag{1}$$

whers

$$G_{un} = 4\pi/\Omega . \tag{2}$$

Alternatively, the gein×area product, MCAG×Ω, may be defined. Due to the finite satallits pointing accurecy, the gain slope must be controlled within the area of uncerteinty for each earth station. Tha arae of uncertainty is called the pointing-error box, aphere or ellipse dependent upon its actual shepa which is determinsd by ths setellite attitude control system. The coverage araa Ω must includa the pointing error.

A pencil beam with a circular foot print is the simplest axample of a beam with an area coverage. If we essume e Geuseien beam ahape and no losses, the power pattsrn

$$G(\theta) = 4\ \ln 10/\theta_{10}\ 10^{-(\theta/\theta_{10})^2} \tag{3}$$

givss the dirsctivity. Tha polar engle θ is measured from the beam axis and θ_{10} is half tha 10-dB beamwidth. The minimum coverage aree gain occurs at tha edga of ths coveraga arae , $\theta = \theta_c$, and is maximized for $\theta_{10} = \theta_c/\sqrt{\ln 10}$. This result also applies for Gaussian beams with elliptical foot prints. Thus, tha minimum coveraga erea gain is about 4.3 dB below paak gain for circular and alliptical foot prints. Tha associatad gain×area product is $4\pi\ 10^{-\ln 10}$ or 15176 degrees^2, which corraspónds to e contourad-beam efficiency of only 36.8 per cent evan though that all lossas heva bean naglectad. This afficiency, which eccounts for the great gain differenca between tha idaal and tha practical global-covarage antenna in Section 1.1, may be improved by a flattar gain over the covarage aree and a staaper gein fall off at tha edge of tha covaraga araa.

When the antenna system providea multipla contourad beams, tha driving antanna paramatar becomas the isolation which can be echiaved betwean beams which re-usa tha same frequency band aithar through spatially separatad copolerizad beams or through orthogonally polarisad beams. Figure 4 illustretes tha differant definitions of intar-beam isoletion which epply for racaiva and transmit satallita antennea. Whan the satellita antanna trensmits, an eerth station sarved by beam B may rscaive en interfaring signal via a sidelobe of beam A. Tha transmit isolation is defined as tha ratio of the dasired signel from beam B to tha undesirad signal from beam A and depends on both the ralativa antenna gein and tha reletive transmit powar, i.e., thu ralativa EIRP. With tha satellite entanna raceiving, tha interferanca occurs via tha sidelobes of tha beam itsalf from earth stations outside the service eree. If all earth stations trensmit with the same EIRP, the raceiva isolation is defined es the retio of the entenna gein towards tha earth stetion in the covarega aree to the antanna gein in the direction of the interfering earth station et the highast sidelobe level. The racaive isoletion is considered to be the most difficult es e single high-level sidelobe which falls in e frequancy re-usa coverege, will destroy the isoletion on ell coverage-erea stations.

The minimum spacing between edjecent copolarised frequency re-usa covereges, measured in beamwidths of the alament beams, datarmines tha required apertura size or resolution of the antenna system. An antenne pointing error of ε will reduce the minimum coverage aree spacing by 2ε. Thus, e lerga pointing arror may requira a significantly larger end more complex antenna system.

2.2. Overview of the Current State-of-the-Art

The INTELSAT communicatione satellites provide en important example of the prectical use of reflector antenna systems with multiple contoured beams. The complexity of in particular the C-band antenna systems have grown significant for each new spacecraft series as illustrated by the increasing complexity of the coverages shown in Figure 5. INTELSAT IV A introduced two-fold frequency re-use through two spatially isolated hemispherical beams by means of an array-fed offset paraboloidal reflector antenne system [8]. This concept was further developed on INTELSAT V where four-fold frequency re-use was realized by the addition of two smaller zone beams in the opposite sense of circular polarization. These zone beams have one shape when the spacecraft operates over the Atlantic or the Pacific Ocean region and another over the Indian Ocean region [9, 10]. The trends towards both more frequency re-uses and more reconfigurability of the beam coverage contours continue on INTELSAT VI. Two hemispherical beams and four zone beams in opposite senses of circular polarization provide six frequency re-uses. The four zone beams are reconfigured for each of the three ocean regions providing a total of 14 coverage beams with six active in a given ocean region [11, 12]. The achievements and the limitations of this technology are summarized in Table 2 [13]. It is common practice to use separate antennas for the transmit and receive function to reduce both the bandwidth over which an antenna is required to operate and problems associated with passive intermodulation.

The increased number of frequency re-uses sets stringent sidelobe and cross-polarization requirements in the order of 27-30 dB over a field-of-view which extends approximately ±10° from the subsatellite point to accommodate both antenna pointing errors and the spacecraft pitch biasing used to maximize the minimum spacing between spatially isolated beams. As the spacecraft are placed above the middle of the oceans, the beam coverages fall near the maximum scan angle so that scan aberrations degrade the achievable sidelobe isolation. So far, however, the diameter of the spacecraft antenna, measured in wavelengths, has been moderate, and the number of beamwidths scanned less than 6-7 half-power beamwidths. This is demonstrated by the observation that for all satellites in the INTELSAT IVA, V to VI series the minimum separation between two copolarized coverages is about 1.5 element-beam beamwidths for 27 dB isolation [14]. This relationship may continue for significantly larger reflector diameters if longer f/D ratios or more complex feed arrays and BFNs can be accommodated to reduce the aberrations of the scanned element beams. Figure 6 shows the calculated contoured-beam efficiency versus coverage area size for INTELSAT VI. The two upper curves apply for a smaller feed element diameter of about 1.3 λ and in case of the uppermost curve also the effect of a slightly increased spacing between the coverage areas [15]. Other contoured-beam antennas also for domestic/regional and direct broadcast systems are reviewed in [16-20].

2.3. Analytic Model of Reflector Element Beams

A simple analytic model is presented for the element beams radiated by small circular or square feeds in an offset paraboloidal reflector with circular aperture. Effects due to the illumination taper and the spillover are included to provide an accurate assessment of the achievable minimum coverage area gain. The model neglects scan aberrations and cross-polarization and is therefore best suited for reasonably large f/D ratios and/or small scan angles. Even then we have found that the model may give surprisingly good predictions for the minimum coverage area gain and the average sidelobe level. The model cannot be used to determine the number of feeds or the feed excitations accurately. Therefore, the model is most useful in initial trade-off studies to determine approximately the antenna size and feed complexity given the coverage specifications. The detailed design optimization should be carried out using element beams calculated by an accurate reflector antenna analysis program such as GRASP [21].

Let the aperture distribution due to a single feed be approximated by

$$g(\rho) = \alpha_o + (1-\alpha_o)[1-(r/a)^2]^n, \tag{4}$$

where the radial variable $\rho < a$. The parameter α_o is the relative illumination at the reflector edge. Typical parameter values corresponding to an element beam would be $n = 1$ and $\alpha_o = 0.7$. We assume that this amplitude distribution applies for all element beams. As we neglect scan aberrations, the phase distributions caused by the lateral displacement of the feeds in the tilted focal plane only direct the wave fronts towards the positions in the beam grid. The element beams are approximated by the normalized patterns

$$f_j(\theta,\phi) = ka\,[\alpha\, A_1(kax_j) + \beta A_{n+1}(kax_j)]. \tag{5}$$

The functions $A_n(x)$ are given by Bessel functions $A_n(x) = 2^{n+1}\,(n+1)!\,J_{n+1}(x)/x^{n+1}$ so that $A_n(0) = 1$. The argument depends on the perimeter ka of the circular aperture in wavelengths and the distance

$$x_j = ((u-u_j)^2+(v-v_j)^2)^{1/2} \tag{6}$$

between the field direction (u,v) and the beam direction (u_j,v_j) in the uv-plane where $u = \sin\theta\cos\phi$ and $v = \sin\theta\sin\phi$. The angles θ and ϕ are the polar and the azimuthal angle in a standard spherical coordinate system directed along the antenna boresight. The pattern parameters α and β in (5) depend via the edge taper α_o upon the primary parameters

$\Delta\theta_3$ - the half-power element beam beamwidth, and
θ_B - the element beam spacing

as outlined below. In order to model the offset reflector and the feed element including spillover losses, the following secondary parameters

d_c/D - the relative offset height or clearance,
d_e - the feed element spacing in wavelengths, and

θ_{10} - half the 10-dB feed beamwidth

are specified. These parameters are indicated on Figure 7. Given the above primary and secondary parameters, the parabola focal length f and the reflector diameter D can be derived. The reflector clearance d_c, the distance from the parabola axis to the reflector edge, should be so large that no scanned beams are blocked by the feed array. The feed element spacing d_e and the feed beamwidth $2\theta_{10}$ are roughly inversely proportional for a given feed type.

Once the above parameters are given, an initial values of the reflector diameter D, the focal length f and subtended semi angle θ^* are calculated assuming a 3 dB edge taper by the approximate formulae:

$$D = 1.029\,(1 - 0.212\,\log_{10}\alpha_o)/\Delta\theta_3 \tag{7}$$

$$d_1 = (0.5 + d_c/D)D \tag{8}$$

$$f = \left(Kd_e/\theta_B + \sqrt{(Kd_e/\theta_B)^2 - d_1^{\,2}}\right)/2 \tag{9}$$

$$\theta^* = \mathrm{Arctg}\; d_1/f - \mathrm{Arctg}\; d_c/2f \tag{10}$$

where K = 0.97. All angles are in radians an all lengths in wavelengths. Note that (9) has no solution if $\theta_B > Kd_e/d_1$. An improved value may now be calculated for the average aperture edge illumination using

$$\alpha_o = 10^{-(\theta^*/\theta_{10})^2/2}/(1 + D^2/8(f^2+D^2)). \tag{11}$$

Given this value, the values for D, d_1, f and θ^* are updated using (7) through (10). The offset paraboloid is now completely determined, and the pattern coefficients are determined from

$$\alpha = \alpha_o/N\,L_{so} \tag{12}$$

$$\beta = (1-\alpha_o)/\left[(1+n)N\right]\,L_{so}, \tag{13}$$

$$N = \left[(1+n+2n\alpha_o+2n^2\alpha_o^{\,2})/(1+3n+2n^2)\right]^{1/2} \tag{14}$$

where

$$L_{so} = 1-10^{-(\theta^*/\theta_{10})^2} \tag{15}$$

gives the element-beam spillover loss. The pattern coefficients are normalised so that the pattern (5) squared gives the directivity. This normalization is convenient for the normalization of the feed excitations discussed in Section 2.5. The effect of typical element-beam edge tapers on the directivity is very small, about 0.1 dB or less. The corresponding element-beam spillover loss is more significant as discussed in Section 2.7. A number of other beam models or simple design rules are available for initial contoured-beam reflector antenna trade-off and layout [22, 23].

2.4 Array Elements

The array element is a key element in determining the overall performance. The feed element must be chosen in accordance with the reflector geometry. For a specified beam-spacing/beamwidth ratio, $\theta_B/\Delta\theta_3$, a smaller feed requires a shorter f/D ratio of the parabola than a larger feed. The $\theta_B/\Delta\theta_3$ ratio is usually close to unity corresponding to an element-beam crossover level of about -3 dB. The feed diameters in the range from 1 to 1.6 λ match well f/D ratios in the range from 0.7 to 1.4. For small f/D ratios, the reflector subtended angle becomes larger and the spillover losses smaller. However, the scan losses increase. The spillover losses are minimized if the product $\theta_{10}d_e$ is kept small. This parameter plays the role of ... array-element quality number and is relatively independent of the size of a particular type of element as already discussed in Section 2.3. For a small circular fundamental-mode horn the value of this parameter is about 1.00 while it is about 1.17 for a small dual-mode or Potter horn. Small corrugated horns are quite useless as array elements because of the large space taken up by the corrugations. From these considerations it would appear that small fundamental mode horn would be the most useful for contoured-beam antenna applications. However, the mutual coupling in the array environment will in practice annihilate the excellent theoretical performance of the small fundamental-mode radiator.

The circular waveguide feed elements discussed above and the square waveguide feed elements are used commonly in circularly polarised antenna systems. Many linearly polarized domestic/regional systems use rectangular feeds of different sizes with or without dielectric loading often illuminating a dual gridded reflector. The feed horn dimensions are optimized to match the image of the coverage area in the focal plane of the reflector. These systems may realise very respectable values of the minimum coverage area gain with a minimum of antenna hardware but are not dealt with in the paper [24, 25].

In a dual circularly polarised antenna, a feed element in conventional waveguide technology consists of a horn radiator, a polariser and an orthomode transducer. In a large antenna system with many feeds, this may be a very bulky and mechanically fragile system. Therefore, microstrip patch radiators have recently received considerable attention as a potential very compact replacement .

2.5 Network Loss and Feed Excitation Normalization

When several feeds are excited simultaneously to generate a contoured beam, the overall edge illumination and spillover loss will in general decrease. On the other hand, the beam forming network (BFN) required to generate the optimised amplitude and phase distribution at the feed ports introduces Ohmic and mismatch losses. This BFN loss increases with the number of feeds ports as more layers of power dividers and longer line lengths are required in the power divider tree. Fully reconfigurable BFNs may have significantly higher losses than fixed BFNs.

The feed excitations a_j must be normalized by

$$P_{in} = 4\pi \sum_{j=1}^{N} |a_j|^2 = \begin{cases} 4\pi & \text{for directivity} \\ 4\pi\, 10^{-LBFN/10} & \text{for gain.} \end{cases} \quad (16)$$

Then, the directivity or the gain will be referred to the total incident power at either the feed apertures or at the BFN input port. The directivity referred to the total radiated power is derived if the excitation normalization is

$$P_{rad} = 4\pi \sum_{i=1}^{N} \sum_{j=1}^{N} r_{ij}\, a_i a_j^* = 4\pi, \quad (17)$$

where r_{ij} is the normalized mutual resistance and $r_{ii} = 1$.

2.6. Mutual Coupling

For a sufficiently large array element with a Gaussian pattern, the normalized mutual resistance is

$$r_{12} = e^{-(kd_{12}\theta_{10})^2/4\ln 10}. \quad (18)$$

This indicates that the mutual resistance depends with the approximations made only on the product $d_{12}\theta_{10}$, which for adjacent feeds is equal to the feed quality number. Thus, the requirements for low mutual coupling and for a small spillover loss are in conflict: A large value of $d_a\theta_{10}$ reduces the mutual coupling but increases the element beam spillover loss. In a study of feed-array directivity, $\cos^q\theta$-approximations to the feed element pattern have been used [26].

The mutual resistance given by (18) is derived from an idealized feed pattern and neglects higher-order modes and cross polarization. It relates to the small signal which appears at the port of a feed when an adjacent feed is excited. This effect is quite negligible for practical feed-array elements and (16) is a good approximation to the power radiated by the feed array. However, the effect of the array environment on the element pattern is much stronger. This effect, which may be termed mutual scattering, sets up the cross-polar mode and higher-order modes at the radiating aperture and has a pronounced effect on the cross-polar performance.

Much work has been carried out on mutual coupling in phased-array antenna systems using the concept of the active element pattern and the unit cell approach. These techniques do not apply to contoured-beam antenna feed arrays which have very non-uniform amplitude and phase distributions. The number of elements is typically smaller than in a phased array and the element size is larger. No electronic scanning takes place and the blindness effects of scanning phased arrays are of no concern. The concept of the embedded element pattern is more useful. The embedded feed pattern is defined as the pattern the feed radiates in the array environment with the feed element excited and all other elements terminated with their actual loads. Mismatches at the feed ports into the BFN have been noted to have a significant effect on the cross polarization - in particular for circular polarization.

A comprehensive study of mutual coupling in contoured-beam antenna feed arrays has been reported in [27]. The method of moments is used and the results apply to a finite number of circular waveguide feeds in a ground plane.

2.7. Spillover Loss Calculation

The spillover loss of a contoured beam will be lower than that of an element beam because of the array factor. The spillover loss is defined as the ratio of the feed power which hit the reflector to the total radiated feed power. The total power radiated by the feed array has been calculated (16). The element beams overlap and are usually not orthogonal. Therefore, the power intercepted and radiated by the reflector must be determined by integrating the total reflector far field. It is much simpler, however, to determine the power radiated by the reflector by integrating the Poynting vector across the reflector aperture A as proposed in [28]. We then obtain for the amplitude distribution in (4)

$$P_{rfl} = 4\pi \sum_{i=1}^{N} \sum_{j=1}^{N} a_i a_j^* \left[\alpha^2 \Lambda_1(kax_{ij}) + 2\alpha\beta\Lambda_{n+1}(kax_{ij}) + (n+1)^2\beta^2\Lambda_{2n+1}(kax_{ij})/(2n+1)\right], \quad (19)$$

where the pattern coefficients α and β are defined above. The parameter x_{ij}, similar to (6), is the spacing between the beam centers in the uv-plane. The "cross correlation" pattern in (19) is wider than the element-beam pattern except in the case of uniform illumination. If the element-beam positions coincide with the nulls of the "cross-correlation" pattern, the beams decouple and become orthogonal. It appear that "losses" due to non-orthogonal beams are of a fundamental nature and may be related to different mechanisms in different antenna systems, e.g., BFN losses, spillover losses in reflector and lens systems and grating-lobe losses in arrays [29].

Figure 8 shows the spillover losses for a single element beam and a cluster of seven element beams. The feed spacing is kept constant equal to 1.07 λ and the beam spacing is increased by decreasing the focal length. The angle subtended by the reflector increases with increasing beam spacing, and the element beam spillover loss decreases. The dotted curve is the element beam spillover loss calculated accurately by a reflector antenna analysis program. The spillover loss of the 7-element cluster is much lower than that of the element beam and almost independent of the beam spacing. For a fixed reflector geometry, the beam spacing (or the beam crossover level) may be varied by changing the feed spacing. Table 3 gives the approximate spillover losses of both single and uniformly excited 7-element clusters of circular fundamental-mode and dual-mode feeds. The table gives the calculated spillover losses for $\theta_B/\Delta\theta_3$ equal to 0.7, 1 and 1.3 corresponding to crossover levels of 1.5, 3, and 5 dB.

	Singls feed			Cluster		
$\theta_B/\Delta\theta_3$	0.7	1.0	1.3	0.7	1.0	1.3
TE_{11}	5.7	3.1	-	1.5	1.3	-
$TE_{11}+TM_{11}$	6.8	4.1	2.3	2.6	2.4	2.1

Teble 3. Spillovar loss in dB.

A significent fraction of the large element-beam spillover for small beam spacings may bs recovered by the erray fector. For the dual-mode feed cluster, where tha greting lobe losses are lerger dus to the larger feed size, the effect of the errey factor on the epillover loss becomes vary emall for lerge beam spacings. A hexagonel errey lattice will reduce the grating-lobe loeses. For each fesd typa, e smaller feed specing will slightly reduce the cluster spillover loss. Ths teble indicates that there is e nead for improved fead alemants which utilize the focel-plene erea mora efficiently but without high mutual coupling. Anothsr end probably more promising remedy might be to use improved reflector eyetems.

Even though the spillover loss of a contoured beam cen be considerebly reducad by the arrey factor, it cen not be naglacted. In the sensa that this loss represents radieted power, it is very harmful in e frequency re-usa entenna system if it is intercepted by ths entenna or by other setellite etructures end re-radiated es cross polarization beck into the coverege or as high sidelobes into edjecent covereges. Such entsnne-farm effscts ere difficult to pradict es thsy depend upon ths wids-angle rediation from the feed array end require spaciel analysis software.

2.8. Scen Charecterietics of Single Raflectore

Figure 9 shows isogain contours for the on-exis end some scenned elemsnt baams for e 3.2 m offset pareboloidel reflector at 4 GHz with en f/D retio of 1.3. Ae e beam is scanned a wey from borcsight, a gein loss end a beem widaning occur. Theee beam degradations depsnd for e given scen angla upon the D/λ retio, the offset engle θ_o, the f/D retio, end the aperture illumination. For the single offset paraboloidel reflector, whars the scen degredation is due to astigmetism [30], the scan loes in dB for the scan engls θ_{sc} may be epproximatad by

$$L_{sc} = C(n,\alpha_o)\ (D/\lambda\ D/f\ \sin\theta_o\ \sin\theta_{sc})^2, \qquad (20)$$

with $C(n,\alpha) = 0.1116[(n+1)\alpha+6(1-\alpha)/(n+2)(n+3)]/(1+n\alpha)$. The peremetars n end α_o are tha axponent end the edge teper of the reflector eperture illuminetion (4). For ecen loseee lerger then 5 dB, (20) predicte too large losses. The ecan loes ie not e loss in redietad power ee the BFN loee end tha spillovar loes. It rapresents e loss in tha resolution or the beam-contouring cepability of the reflector due to the widsning of the alement beems for large scan anglee. Some scen degredation may be compeneetsd for by a more complex fesd arrey.

The scan loeses of the csnter-fed peraboloidal raflector ere for tha eame apertura diemeter, f/D retic, scen engle end eperturs illuminetion order of magnitude less then those of the offset-fed reflector. The dominent eberretion is due to coma, which hee e minor impect on scen loss end mainly degredes the sidelobe performance [31]. As the totel scen loss is determined by e combinetion of coma, highsr-order estigmatism end sphsricel eberration, no simple expreeeion exists for ths scan loee in the canter-fed pareboloidel reflector.

2.9. Polerizetion Consideretions

Circuler polerisetion wes initielly chosen for use in the internetionel communicetione satellite system beceuse of the Fereday rotation. When e linearly polerized signel traversee the ionosphere, the polerisetion plene undergoes e rotetion. At 4 end 6 GHz, the maximum Feraday rotation is epproximately 9 and 4^o with opposite directions for transmit end receive (CCIR Report 551-1, Sect. 2.3.1). This choice of polerisetion wes fortunete from the point-of-view of entenne technology. Circularly polerized offset reflectors do not generete cross polerisetion but exhibit e slight beam squint in the plene perpendiculer to the plene of symmetry [32, 33]. The magnitude of this beam squint is given by the epproximate formula

$$\Delta\beta = \mathrm{Arcsin}(\lambda \sin\theta_o/4\pi f). \qquad (21)$$

The direction of the beam movement depends upon the hend of the polerisetion. The Fereday rotetion is inversely proportionel to the squere of the frequency end presents no problem ebove 10 GHz. Then, depolerisetion ceused by rain becomes importent end from the point-of-view of cross polsrisetion, circuler polerisetion becomes the worst possible choice. The shape of rein drops is generelly sphericel. However, the ehepe of felling rein drops becomes slightly ellipticel due to the eir resistence. The rein-induced ettenuetion end phese shift ere maximum (minimum) for the polarisation eligned with the major (minor) exis of the rein drop. No depolerisetion tekes place for linear polerisetion eligned with the major or the minor axis of the rein drop. In practice, the depolerisetion is minimised for linear polerisetion eligned with locel earth station verticel end horisontel (CCIR Report 564-2, Sect. 8.2). Thus for frequency re-use entenne systems in the 14/11 GHz bands end possibly even the 30/20 GHz bands, linear polerisation should he used aligned with the everege locel verticel end horisontel within each coverege eree [34]. However, this elignment will reduce the cross-poler isolation between edjecent coverege ereas under clear-sky conditions es the polerizetions then no longer ere orthogonal.

In the single offset pareboloidal reflector, the feed exis is in generel tilted to bisect the engle subtended et the focel point by the reflector in its plene of symmetry. This feed exis tilt generetes two cross-poler lobes in e linearly polerised system [32, 35, 36]. The peak of the cross-poler lobes occurs in the plene perpendiculer to the plene of symmetry. For e uniformly illuminated eperture, the peak cross-polar level reletively the peak copolar level is

$$E_{cross}/E_{co} = 0.36\ \theta^*\ \tan\theta_o/2, \qquad (22)$$

where θ^* (in radians) is the semi angle subtended by the reflector. A tapered aperture illumination will decrease the cross polarisation slightly. Any significant reduction requires either a more complicated feed element, a more complex feed array design, or that a gridded reflector be used.

3 OPTIMIZATION OF CONTOURED-BEAM REFLECTOR ANTENNA SYSTEMS WITH FEED ARRAYS

The synthesis of a contoured-beam antenna system may be divided into steps. Initially the fundamental antenna performance requirements such as

- coverage area(s),
- minimum coverage-area gain,
- maximum coverage-area gain slope,
- sidelobe and cross-polar isolation and
- frequency band

must be specified. Next, the antenna designer may identify the range of a number of antenna parameters such as

- reflector aperture size, and
- feed-array complexity

and examine the performance trade-offs versus the antenna system size and complexity. These trade-off studies require that optimum feed excitations be determined and the resulting contoured beams be analyzed for several antenna configurations. If these studies are carried out with simple analytic element-beam models, large savings can be realised in both human effort and computer time.

When a viable solution has been identified by these initial optimizations, an element-beam layout with half-power element beam beamwidth $\Delta\theta_3$ and the element beam spacing θ_B will be known. Given this element-beam grid, the feed-element size and the orientation of antenna on the satellite, an initial reflector antenna and feed array layout may be determined ensuring that no blockage occurs. Then, the detailed optimizations are carried out using element-beam data determined by an accurate reflector antenna analysis program. It is desirable to include as many potential error sources as possible. Degrading effects not predicted by the software can be included by means of measured data, e.g., of the patterns of the feeds embedded in the array. In case the results of the optimisations indicate that the performance requirements can not be met, these requirements or the range of antenna parameters being considered must be revised.

3.1 Optimisation Procedures

Many different, more or less rigorously based optimisation procedures have been proposed to determine the feed excitations which provide the "best" contoured beam. It appears that no optimisation procedure is complete. Usually the antenna designer specifies the reflector and the feed array geometry. Only then an optimization procedure determines the "best" feed excitations by optimisation of the antenna performance, e.g., gain and isolation, over a finite number of pattern sample points. These sample points will be termed synthesis stations as they may not correspond to actual earth stations. A more complete optimisation can be carried out by repeating the feed excitation optimisation for a large number of antenna geometries. A general optimisation procedure may optimise both element-beam grid and excitations but the usefulness of the results will be limited by the accuracy of the element-beam model. For practical antenna systems, it is still prohibitive and probably not desirable to include in the closed optimisation loop a complete electromagnetic analysis with a.o. BFN tolerance analysis and feed-array mutual coupling analysis.

A contoured-beam synthesis is a power-pattern synthesis problem as opposed to a field-pattern synthesis problem. Furthermore, the power pattern are only specified in certain regions. The power pattern in the complementary regions of the far-field sphere and the phase pattern should be allowed to float in the optimisation and take on any values which improve the power pattern in the regions of interest. Thus, even the apparently simple problem of determining the best feed excitations for a specified antenna geometry is a complex nonlinear problem and it can not be determined if a solution is a local or a global optimum. It appears often, however, that the optimum is quite flat so that small changes in antenna geometry, initial feed excitations input to the optimisation procedure, stations locations, etc. may result in quite different feed excitations but very often only in small changes of the antenna performance. It is recommended to input different initial solutions to iterative optimization algorithms and to carry out sensitivity studies of the final solution with respect to excitation errors. The optimization is in general carried out on the copolar field only. In systems which implement frequency re-use by means of orthogonal polarizations, the required cross-polar performance is typically implemented by antenna designs which have low inherent cross polarization.

The following four sections describe a least-squares optimisation procedure with a power constraint, the formulation of the minmax synthesis problem, a minmax optimisation procedure which utilises a general-purpose algorithm which recently has been extended to work more efficiently on contoured-beam synthesis problems, and recent progress with minmax or maxmin algorithms which have been developed specifically for contoured-beam reflector antenna synthesis. Many different approaches are described in the literature [e.g., 37-45].

3.2 Least-squares Synthesis

The method, also known as the regularisation method, is explained below using a matrix notation [46]. We define the matrix $e = \{e_{ij}\}_{M \times N}$ where e_{ij} is the contribution of element beam j, $j = 1,2,\ldots,N$, towards synthesis station i, $i = 1,2,\ldots,M$. Two column vectors $a = \{a_j\}$ and $g = \{g_i\}$ contain the N excitations and the desired field on the M synthesis stations. The number of synthesis stations exceeds in general the number of element beams and a solution can only be found in a least-squares sense. In order to optimize the minimum coverage area gain, the power input to the antenna must be constrained. Therefore we add the norm of the excitation vector e, which gives the incident power (16), to the least-squares pattern error by a Lagrange multiplier α. The expression to be minimised is then

$$J = (e^T e^T - g^T)W(ea - g) + \alpha e^T e, \tag{22}$$

where the weight matrix W is a diagonal matrix and the superscript "T" denotes conjugate transposition. This gives the following matrix equation for the unknown excitations e

$$(e^T We + \alpha)e = e^T Wg. \tag{23}$$

Initially, we only specify the amplitude of the desired field on the synthesis station by

$$g_i = (G_o p_i f_{oi})^{1/2}, \tag{24}$$

where G_o is a gain normalisation constant, p_i the desired relative gain level, and f_{oi} a path length correction factor if flux density rather then gain shall be optimized. As gain normalisation constant we can use the peak achievable minimum coverage area gain (1) with a back off. This requires that the angular area Ω of the coverage area be determined.

The relationship between the Lagrange multiplier α and the incident power is established by means of the eigenvalue equation corresponding to (23). The matrix $e^T We$ is Hermitian and the positive real eigenvalues and the eigenvectors may be determined by standard techniques. We expand the unknown excitation vector in the complete basis formed by the eigenvectors. The expansion coefficients are determined in terms of the Lagrange multiplier α which in turn is derived from the power constraint (16).

The specification of the desired field (24) implied a constant pattern phase. To remove this limitation in a heuristic way we include a phase factor $\exp(j\Phi_i^k)$ which is updated iteratively. At the kth step we determine the pattern phase from the excitations derived in the k-1th step by

$$\exp(j\Phi_i^k) = \sum_{j=1}^{N} a_j^{k-1} e_{ij} / \left| \sum_{j=1}^{N} a_j^{k-1} e_{ij} \right|. \tag{25}$$

A new right-hand side of (23) is calculated and a new value of α must be determined for each step in the phase iteration. However, the eigenvalues and the eigenvectors remain the same throughout the iteration. The iteration is terminated when the relative change of the least-squares error (22) decreases to a specified value.

3.3 Formulation of Minmax Synthesis Problem

The least-squares solution discussed above will in many cases be very good except, possibly, on a few critical synthesis stations. A minmax method may improve the performance on the these critical stations generally at the expense of the average performance over all stations. The minmax optimisation problem consists of finding the feed excitations e_j so that the realised power gain

$$pw_i = \left| \sum_{j=1}^{N} a_j e_{spj} \right|^2 \tag{26}$$

minimizes the maximum value of the residual or pattern error

$$f_i = w_i \left| pw_i/(f_{os}G_o) - p_i \right| \tag{27}$$

over all pattern constraints i, i.e., synthesis stations s and polarisations components p. In (26) and (27), the following notation has been used

- e_{spj} field towards station s in polarisation p from element beam j,
- f_{os} path length compensation factor towards station s if flux density is optimised,
- p polarisation selector equal to 1 or 2,
- p_i desired relative power level for pattern constraint i. Often p_i = 1 for coverage-area constraints, p_i = 0 for isolation constraints and p_i equal to a specified gain roll-off function with a back off if a reference pattern shall be enforced,
- s synthesis station number, $s = 1,2,\ldots,M_s$, and
- w_i weight factor used to equalise coverage and isolation constraints.

The residuals for coverage area pattern constraints which exceed the gain goal are set equal to zero.

The minmax optimisation problem consists of determining the feed excitation vector e which minimizes the maximum residual

$$F_{minmax} = \max_i f_i. \tag{28}$$

The corresponding least-squares error (22) minimises the average deviation over all stations. The weight factors w_i and W_i are used to increase the magnitude of the residuals in isolation areas to correspond to the magnitude of the copolar residuals in the service area. If the minimum coverage area gain is MCAG, the maximum sidelobe (cross-polar) level is MSL and the coverage area weight factor is unity, the minmax sidelobe (cross-polar) weight factor

$$w = (G_o\text{-MCAG})/\text{MSL} \tag{29}$$

will equalise the residuals. The weight factors behave slightly differently in the minmax and in the least-squares optimisation. The best agreement between the two optimisations is obtained if $W_i = w_i^{1/2}$.

3.4 Synthesis by General Minmax Algorithm

The general minmax algorithm is an extension of the iterative method described in [47]. Let the column vector x_k represent the excitation vector at the kth step of the iteration, $f_i(x_k)$ the associated error or residual (27) at the ith pattern constraint, the column vector b_{ik} an approximation to the gradient of the residual with respect to the excitations and the column vector h an increment to the excitation vector. Then,

$$F_k(h) = \max_i \, (f_i(x_k)+b_{ik}^T h) \tag{30}$$

is a linear approximation of the minmax pattern error (28) for small values of $\| h \| = \max|h_j|$. At each step of the iteration, the linear subproblem (30) is solved by linear programming subject to a bound on the solution, $\| h \| < \lambda_k$, giving the solution h_k. The vector x_k+h_k is accepted as the new approximate solution if the non-linear objective function has decreased. Otherwise the step is rejected and repeated with a smaller λ_k. The bound λ_k reflects the region near x_k where (30) is a reasonable approximation to the original non-linear problem and it is adjusted automatically during the iteration. The approximations to the gradients are updated using a rank-one formula by Broyden [48],

$$b_{ik+1} = b_{ik}+(f_i(x_k+h_k)-b_{ik}^T h_k)/(h_k^T h_k)h_k. \tag{31}$$

In a contoured-beam optimization, the number of synthesis stations can be large in particular when a global envelope constraint in enforced as in Section 4.2 or when several contoured beams with common excitations are optimized simultaneously as in Section 4.3. A significant amount of storage is needed for the derivative matrix and large linear programming problems must be solved at each step of the iteration. In practical problems, however, the number of stations where the pattern error (residual) attains the maximum value is small compared to the total number of stations. Therefore at each step, we identify the stations within a specified range of the largest residual. These stations define the overall pattern error F in a neighborhood about x_k and are called the active stations. Working mainly only with the stations within a range of the largest residual, we realize large savings in storage and computing time whereas the convergence properties remain the same. The derivative matrix is stored and updated only for the active stations - typically about 1/5 and less of all stations. The size of the linear programming sub problems are reduced by the same proportion. However, all stations are still checked at each step of the iteration and the active set is updated as required. The gradients of the residuals which are active at both x_k and x_k+h_k are updated by (31). For the newcomers we use a difference approximation since we have no estimate b_{ik} of the gradient at x_k.

In case of a singular problem, the iteration may become slow because the process is caught in a long valley with steep sides [49]. It is a characteristic of a singular problem that with N excitation variables, the number of worst stations where the residuals are equal to the maximum residual will be less than N+1. The number of worst stations is generally considerably less than the number of active stations used in the iteration and less than the number of excitation variables even in the final stages of the iteration. Thus, most contoured-beam synthesis problems appear to be singular. When we decide that the process has been caught, we apply a "special" non-descent iteration to bring the process out of the valley. It can be proven that the extended method theoretically has the same convergence properties as its processor whereas in practice the new method is considerably faster and can handle much bigger problems within the same computer memory.

3.5 Specialized Minmax Algorithms

The general minmax algorithm provides the maximum degree of freedom in the design. We may choose to optimize only the amplitudes, only the phases or both the amplitudes and the phases of the excitations with only small changes of the software. Also, the location of the element beams may be optimized or degrading affects such as BFN frequency dispersion and BFN random errors could be accounted for. However, the general algorithm does not take advantage of the special properties of a specific contoured-beam synthesis problem as opposed to, e.g., microwave network synthesis problems. The general algorithm does not use the closed-form analytic derivative of residuals which are available in special cases but uses approximations derived by finite differences and Broyden's formula. These approximations are both more time consuming and more inaccurate. They may result in a reduced rate of convergence in the final stages of the iteration, where a large linear programming problem may have to be solved at each step.

A simple minmax algorithm has been proposed by in [50] to be applied in cases with amplitude only or both amplitude and phase excitation optimization. For the excitation normalization (16) with no loss, the derivative of the ith residual f_i (27) with respect to a_j is given by

$$f_i{}'_j = 2[(\sum_{j=1}^{N} a_{ij} e_j) a_{ij}^* - |\sum_{j=1}^{N} a_{ij} e_j|^2 e_j]. \tag{32}$$

The factor $w_i/(f_{oi}G_o)$ has been suppressed. It is further shown in [50] that the gradients ∇f_i are perpendicular to the excitation vector. At each step in the iteration, the active stations are identified and a best search direction is found by solution of a system of linear equations. The length of the incremental vector Δe_k to be added to the excitation vector e_k in the kth step is determined very efficiently by a linear search.

We found that each step in the iteration proceeds extremely fast compared to the general minmax algorithm and that very often good results are obtained. The range of the residuals which define the active stations gradually decreases during the iteration. In our implementation, the method sometimes requires very many iterations to terminate. When the number of active stations becomes equal to the number of excitations, the linear system of equations used to determine the search direction becomes singular and the iteration is forced to terminate.

Recently, the convergence of the method has been considerably improved by determining the best search direction by solving a linear programming problem and improving the linear search [51]. Only the worst stations are considered in the search direction determination. The results indicate that order-of-magnitude saving in computer time may be realized when closed-form derivatives are used instead of derivative approximations. A possible future extension may be to implement a hybrid algorithm which would use analytic derivatives whenever they are available and derivative approximations otherwise.

4 SYNTHESIS EXAMPLES

The optimisation procedures described in Section 3 have been implemented in a synthesis software. This section gives three examples of results obtained with this software package. Other recent design examples includes dual-mode antenna optimisation [52] and an offset side-fed Cassegrain antenna with ten contoured beams [53].

4.1 Antenna without Stringent Sidelobe Specifications

4.1.1 Contoured-beam antenna specifications

The optimization of a contoured-beam reflector antenna system for a European Communications Satellite coverage is provided to illustrate the design procedure. The antenna is a transmit antenna with the requirements outlined below:

Frequency band:	10.7-11.7 GHz
Polarisation:	RHCP
Min. coverage area gain including BFN loss and spillover:	28 dBi
Max. pattern slope in coverage area:	5 dB/degree
Max. copolar sidelobe level:	-20 dB
Min. cross-polar isolation in coverage area:	30 dB

An area coverage including a 0.2° pointing error was specified. The number of feeds was anticipated to be between 20 and 30 and the antenna envelope should be compatible with the ECS platform and the Ariane launcher. The feed element was chosen to be a small conical horn placed in a hexagonal grid with an element spacing of 1.07 λ at the center frequency. The coverage was composed of four isolated stations and a large area specified by a piece-wise linear contour. The area specification was converted into discrete station specifications by adding synthesis stations inside the piece-wise linear contour. It was found that a spacing between the samples in the uv-plane of

$$\delta_{uv} = 0.01\,\Delta\theta_3, \tag{33}$$

with the element beam beamwidth $\Delta\theta_3$ in degrees, gave a reasonable trade off between accuracy and computation time. This corresponds to about 60 per cent of the maximum Nyquist sampling spacing λ/D and allows for truncation effects near the edge of the coverage, the tilt of the effective aperture plane along the plane of the reflector rim curve, etc. When a large range of element beam beamwidths is being considered, it becomes necessary to use more than one coverage sampling spacing. Figure 10 shows the 58 synthesis stations representing the ECS coverage for the half-power beamwidths 2° and 1.5°. The spacing (33) between the internal samples is 0.015 corresponding to 0.86°. For the half-power beamwidth equal to 1.2°, the sample spacing was reduced to 0.012 or 0.69°, and 81 synthesis stations were obtained.

4.1.2 Initial optimisation with analytic element beams

The preliminary design trade-off was carried out with the analytic beam model for the beamwidths $\Delta\theta_3$ = 2.0°, 1.5° and 1.2° to determine approximately the reflector size and the number of feed element. In each case, the beam spacings θ_B = 1.2, 1.1 and 1.0 $\Delta\theta_3$ were considered. The initial beam grids set up included all element beams with a distance less than Δ_{BS} from the nearest stations. With Δ_{BS} = 1.25, 1.00 and 0.80 θ_B, a total of 27 initial beam grids were considered. In each case, the flux densities on the Earth were optimised taking into account the path length differences between the satellite and the synthesis stations. An initial set of real excitations was obtained by the least-squares algorithm and used as starting point for the minmax algorithm which also varied the antenna pointing and the beam lattice orientation and spacing. All the excitations are real-valued because the element beams are real-valued.

The configuration with $\Delta\theta_3$ = 1.5°, Δ_{BS} = 1.65° and initial value θ_B = 1.65° was found to give the best compromise between antenna complexity and performance. However, the optimum is quite flat. Figure 11 shows optimized the element-beam lay-out, which includes 24 element beams, and the isogain contours of theoptimised contoured beam 1, 2, 3, 5, 10, 15, 20, 25, and 30 dB below peak gain. The number of "active" stations in the minmax optimisation is 17, which is well below 24, the number of element beams. This indicates that we are dealing with a singular problem. Only four least-squares residuals exceeded the minmax residual. The associated synthesis stations belonged to the set of "active" stations in the minmax solution. The analytic beam model provides an initial antenna geometry shown in Figure 12 as seen from the dish. The feed lay-out is the image of the element-beam lay-out in Figure 11.

4.1.3 Final optimisation with PO/GTD element beams

The initial antenna geometry was further optimised using accurate element beam data determined by PO, GTD and Whittaker reconstruction. These beams are complex-valued so that both feed excitation amplitudes and phases were optimized. The initial least-squares feed excitations were determined using iterative updating of the pattern phase and used as starting point for the minmax excitation optimisation. The optimised excitations were inspected for weakly excited feeds. These feed were eliminated and the excitations of the remaining feeds re-optimized. Table 4 summarises the principal results with an assumed BFN loss of 1.4 dB.

	Least-squares Min flux	Minmax Min flux	Minmax Min gain	Spillover
Analytic beam model:				
all 24 beams	27.85	28.31	28.09	-1.02
PO/GTD beams from GRASP:				
all 24 beams	28.21	28.40	28.17	-1.21
-beams 18, 20 and 22	27.81	27.97	27.73	
-beams 20 and 22	28.15	28.26	28.02	

Table 4. Results of ECS optimizations. Levels in dB and dBi.

Several observations may be made. Firstly, the least-squares solution is in all cases quite good compared to the much more time consuming minmax solution. Secondly, the prediction obtained by analytic element-beam model is very close to the one obtained using a much more accurate element-beam model. The element-beam model is quite sensitive to the value assumed for the feed quality number $d_e 8_{10}$. Thirdly, deleting feed or element beam 18 has a significant impact on the solution so that caution should be exercised when feeds are eliminated. The optimization should begin with a generous number of feeds which gradually are removed. Each time, the excitations of the remaining feeds must be re-optimized. Figure 13 and 14 show the element beam half-power contours and the contoured-beam isogain curves derived by means of PO, GTD and Whittaker reconstruction at 10.7 and 11.7 GHz. The decrease of element-beam half-power beamwidth with increasing frequency may be noted. The agreement with the analytic beam model in Figure 11 is good except for a slight widening of the low level contours in Figure 13 and 14 due to the scan aberrations neglected in the analytic element beam model.

The finite tolerances of the BFN, mismatches, frequency dispersion in the BFN and mutual coupling will cause the realized feed excitations to deviate from the optimum values determined by the synthesis software. Excitation errors not accounted for will degrade the antenna performance. Some of the degrading effects may be included in the pattern optimization. Thus, it has become common practice to carry out the excitation optimization simultaneously at both edges of the frequency band if the antenna is required to operate over any significant bandwidth. Table 5 summarizes the results of computer simulations of the effect of random excitation errors on the minimum coverage area gain. For the range of errors and the configuration considered, amplitude errors seem to be more serious than phase errors. For practical applications, the average excitation error should be less than a few tenth of a dB in amplitude and 5° in phase.

Peak excitation amplitude error	Peak excitation phase error	Gain degradation due to amplitude only	Gain degradation due to phase only	Gain degradation due to amplitude and phase
0.3 dB	3°	0.19 dB	0.00 dB	0.17 dB
0.6 dB	6°	0.32 dB	0.09 dB	0.44 dB
0.9 dB	9°	0.61 dB	0.16 dB	0.66 dB
1.2 dB	12°	1.16 dB	0.24 dB	0.88 dB
1.5 dB	15°	1.12 dB	0.32 dB	-

Table 5. Degradation of the minimum coverage area gain as a function of random excitation amplitude and phase errors.

4.1.4 Measurements on array-fed contoured-beam antenna

In the European Space Agency's COBRA (contoured-beam reflector antenna) program, the prototype of the antenna described above was designed, manufactured, integrated and tested [54]. The rms deviation of the measured amplitude and phase excitations from the nominal values are indicated in Table 6 at the edges and the center of the frequency band.

Frequency	Amplitude	Phase
10.7 GHz	0.58 dB	5.6°
11.2 GHz	0.24 dB	5.9°
11.7 GHz	0.59 dB	6.5°

Table 6. Rms deviations of excitations at feed ports.

Figure 15 shows in full line the measured copolar contours 1, 3, 5, 10, 15 and 20 dB below peak gain at the edges and the center of the frequency band. The calculated contours 3 and 20 dB below peak gain are superimposed in dotted line. The agreement is fair apart from 11.7 GHz where strong mutual coupling effects between the small circularly polarised feeds not accounted for in the analysis are believed to degrade the minimum coverage area gain from 28.1 to 25.6 dBi at Barcelona. The cross-polar discrimination was better than 28 dB at the design frequency [55].

4.2 Impact of Global Sidelobe Constraint on Frequency Re-use Antenna System

The interference between the different satellite communications systems has in the past been controlled by coordination such that any new system would not obstruct the existing systems. In the future, it likely that communications satellite antennas must meet reference pattern specifications similar to those which already apply to earth-station antennas and direct-broadcast satellite antennas. This will conserve the finite available frequency bandwidth and geostationary arc. Such antenna reference patterns are difficult to define for a contoured beam, which may be of a complicated shape. They will complicate the antenna design process as many more synthesis stations must be considered. This example investigates the potential impact of a global pattern envelope constraint on an antenna similar to the Intelsat VI 4-GHz hemi/zone antenna already considered in Section 2.2. This antenna already meets stringent sidelobe requirements in the adjacent frequency re-use coverage areas.

4.2.1 Sidelobe envelopes of current antennas

Figure 16 shows the calculated isogain contours at MCAG (the minimum coverage area gain) and 27, 30 and 33 dB below MCAG for the Intelsat VI Indian Ocean region (IOR) zone 2 beam at the lower edge of the 4-GHz band where the problems with sidelobes and the roll-off of the pattern from the coverage area are the most severe. The four spatially isolated zone beam coverages are indicated by the four piece-wise linear composite coverages. We note that fairly high sidelobes extend from zone 2 towards zone 4. The figure also shows a number of linear segments which extend from about 1^{o} inside the zone beam coverage to about 7^{o} outside. Figure 17 shows the superimposed cuts along these gain roll-off pattern traces. The horizontal angular scale gives the distance from the point where a gain roll-off pattern trace intersects the MCAG contour. No traces away from the Earth are considered. In these directions, the sidelobes are much higher. The full (dotted) line near 0^{o} represents the maximum (minimum) envelope of the pattern traces. The full (dotted) line further away indicates the envelope of most (all) of the traces. The dot/dash line indicates the additional degradation caused by the calculated line length dispersion in the beam-forming network. In a practical antenna, several other imperfections will degrade the performance.

4.2.2 Gain roll-off optimization

Figure 18 indicates the location of the synthesis stations used in the optimization. Initially, no gain roll-off stations (indicated by 7) were used. The optimization then uses 176 stations and 36 beams. It is carried out at both band edges simultaneously so that the number of pattern constraints is twice the number of stations. Figure 19 shows the resulting gain contours at the lower edge of the band with isogain contours at the MCAG level and 27, 30 and 33 dB further down. The levels do not include losses and give directivity. The minmax solution is superior to the least-squares solution on the worst stations and improves in this case the MCAG level by 1.2 dB. The sidelobes are higher than in Figure 16 but the fit to the desired composite coverages is tighter.

Figure 20 shows the optimized gain contours obtained for carefully selected sets of gain roll-off stations. Initially, gain roll-off stations were set up from the edge of the composite coverage with a maximum tolerable field level calculated from a gain roll-off reference curve. This may lead to the specification of critical synthesis stations which with the minmax algorithm would destroy the overall antenna performance. With the gain roll-off curve used in the optimization, it was found that no gain roll-off station should be placed closer to the coverage area than 3^{o} for this zone beam. Also, no stations should be placed in (the polar) regions where no feed is available for controlling the pattern. The resulting 265 synthesis stations are shown in Figure 18 with deleted gain roll-off stations marked by circles. The sidelobe performance has been considerably improved while the MCAG level has been reduced by only a few tenth of a dB. However, the gain slope of the edge of coverage has been degraded. Increasing the number of feeds slightly will improve the MCAG level and the gain slope but seem to have little impact on the sidelobe performance.

4.3 Reconfigurable Antennas with Shared Excitations

Increasing satellite lifetimes of 10 to 14 years have accelerated the need for the same spacecraft to be able to provide different services over different coverages at different times. The full range of possible future requirements to a spacecraft cannot be anticipated for such a long time and can probably only be met by a fully reconfigurable antenna system. Such antenna systems do not require any special synthesis software as the antenna may be optimized separately for each coverage requirement. However, they are excessively complex and expensive to implement, and in practice, less complex and more reliable systems with limited reconfigurability are implemented, e.g., as in the Intelsat C-band hemi/zone antenna systems by means of switches. Such a case is considered in this section. A set of shared excitations is optimised to meet the Intelsat VI Atlantic and Indian Ocean region zone 2 beam coverage requirements. The shared excitations would then by switches be combined with separate sets of unique excitations for each ocean region. In each ocean region, the sidelobe requirements in the adjacent zone beam coverages are included.

Figure 21 and 22 show the 185 synthesis stations used for the Indian Ocean region zone 2 beam optimisation and the 218 synthesis stations used for the Atlantic Ocean region zone 2 beam optimisation. The minimum coverage area gain is optimized subject to meeting a sidelobe isolation of more than 30 dB in the adjacent zone beam coverages. First, the two zone beams will be optimised independently of each other. Then, the two zone beams will be optimised simultaneously sharing many element beams with identical excitations.

4.3.1 Optimisation with separate excitations

A initial optimisation is carried out for each coverage separately. Figure 23 and 24 show the contour plots of the two optimised zone beams. The optimizations are carried out using the analytic element-beam model. Isogain contours are shown through the minimum coverage area gain level and 20, 25, 30 and 35 dB further down. The minmax pattern error is slightly larger for Indian Ocean region zone beam.

4.3.2 Optimisation of shared excitations

At this stage, the two sets of excitations obtained by the optimization of each ocean region separately are inspected and each excitation is assigned to one of the following three BFNs:

BFN 1 generates the excitations only used by the Indian Ocean region zone beam,

BFN 2 which generates the excitations only used by the Atlantic Ocean region zone beam, and

BFN 3 which generates the excitations which are shared for the two zone beams.

The total number of element beams is 46. The breakdown of the element beams and the excitations between the two zone beams and the three BFNs is given in Figure 25. The combined synthesis problem consists of 61 different excitations and 403 synthesis stations. In this case, the synthesis is carried out so that the power division between BFN 1 and BFN 3 for the Indian Ocean region zone beam and between BFN 2 and BFN 3 for the Atlantic Ocean region zone beam are optimized by the program. Figure 26 and 27 show the contour plots of the two optimised zone beams with shared excitations for the analytic element-beam model. The minimum coverage area gain (or rather directivity) and the minimum sidelobe isolation are listed in Table 7 for the case with separate excitations and with shared excitations. The table gives data obtained both with the analytic element beams and with element beams calculated by an accurate reflector analysis program.

	Analytic element beams		PO/GTD element beams	
	Separate	Shared	Separate	Shared
Min. gain:				
Indian 2	26.18 dBi	26.19 dBi	25.91 dBi	26.00 dBi
Atlantic 2	25.58 dBi	25.36 dBi	25.32 dBi	25.17 dBi
Min. isolation				
Indian 2	33.09 dB	33.10 dB	32.29 dB	32.55 dB
Atlantic 2	33.81 dB	33.10 dB	33.09 dB	32.55 dB

Table 7. Performance with separate and with shared excitations.

Thus, no degradation has taken place for the Indian Ocean region zone beam which had the largest minmax residual. The performance of the Atlantic Ocean region zone beam has been "equalized" so that minmax residuals now are identical for the two zone beams. The agreement between the results obtained by analytic beams and PO/GTD beams is surprisingly good.

5 SHAPED CONTOURED-BEAM REFLECTOR ANTENNAS

In this Section we consider an alternative contoured-beam reflector antenna requiring only a single feed. The surface of the offset reflector is shaped so that the modified wavefront along the original reflector surface provides the desired wavefront. The deviation from the paraboloidal surface is so small that the amplitude distribution along the original reflector surface remains essentially undistorted and only negligible cross polarisation is generated. The similar surface shaping technique has previously been utilized for a Japanese experimental Ka-band communications satellite [56, 57].

5.1 Optimisation of Aperture Phase Distribution

In our version of the synthesis technique, the phase of the aperture field is expanded into Zernike or circle polynomials, i.e.,

$$\Phi(\rho,\phi) = \sum_{n=1}^{N} \sum_{m=-n}^{n} c_{mn} e^{jm\phi} R_{mn}(\rho), \qquad (34)$$

where ρ and ϕ are the polar aperture coordinates and $c_{-mn} = c_{mn}^{*}$. The Zernike or circle polynomials find use in optics for orthogonal expansions in circular apertures. The polynomials are simply related to the scan aberrations such as spherical aberrations, astigmatism, coma, etc. [59]. Rapid calculation of circle polynomials is possible by recursion. The expansion coefficients c_{mn} take the role of the feed excitations in the array-fed reflector. For a particular set of expansion coefficients, the field is calculated on all stations by a simplified and fast physical-optics integration across the deformed reflector surface. The general minmax routine described in [47] is used to determine an set of expansion coefficients which optimise the gain on all synthesis stations. The procedure has also been utilised to synthesise elliptical beams with very low sidelobes [58].

When an optimum phase distribution has been determined, the shaped reflector is derived by a ray-tracing procedure from the offset paraboloid used as initial solution. The optimisation of the phase expansion coefficients is numerically more difficult than feed excitation optimisation. The element beams are almost orthogonal and varying one feed excitation affects only few stations. The phase expansion coefficients, on the other hand, interact nonlinearly and varying one coefficient will affect all stations but by very small amounts.

The reflector shaping procedure has been applied to the ECS coverage already considered in Section 4.1. The design was carried out at 11.2 GHz using the offset paraboloidal reflector similar to the one considered in Section 4.1 as starting point. An optimized surface deformation which generates the contoured beam is indicated by the three-dimensional plot in Figure 28. The optimised shaped reflector antenna system was analysed by physical optics. Figure 29 shows the calculated copolar isogain contours at the edges of the frequency band 1, 2, 3, 5, 10, 19, 20, 21 and 30 dB below peak gain. The calculated minimum coverage area directivity of 28.81, 29.21 and 28.84 dBi at 10.7, 11.2 and 11.7 GHz compare favorably with the corresponding minimum coverage area gain values of 27.93, 28.18 and 28.10 dBi of the array-fed reflector. No attempt was made to suppress the sidelobes. The antenna was assumed to be circularly polarised. The cross-polar performance was found to be very sensitive to the cross-polar performance of the feed. Even low levels of feed cross polarisation would generate "hot spots" of cross polarisation in the reflector far field.

5.2 Measurements on Shaped Contoured-beam Reflector

The shaped reflector contoured-beam reflector was re-optimised with a smaller offset angle θ_o to allow the use of a linearly polarised feed horn which was available. A modified aperture phase expansion was determined with significantly lower sidelobes at the cost of a reduced minimum coverage area gain. The shaped reflector was manufactured for the scaled frequency band 16.4 - 18 GHz in order to reduce the reflector size to be within the limitations set by the surface machining equipment available. The antenna measurements were carried out at the spherical near-field test range at the Technical University of Denmark. During the antenna measurements, the feed horn was found to move and it was necessary to strengthen the feed support etructure. Figure 30 compares over an extended engular renge the meeeured end the calculated co- and croee-poler pattern cuts along the planes of maximum end of minimum beamwidth. The agreement is excellent apart from the engular region $7^\circ < \theta < 14^\circ$ in the plane of the narrow beamwidth, where scattering from the enlarged faed support etructure appeers. The measured minimum coverege eree directivity of 27.3 dBi occurs at the high end of the band where the predicted velue ie 28.1 dB. The ehaped reflector antenna holds significent advanteges over the array-fed reflector antenne for applicetione where no reconfigurebility and only e eingle beam is required. No BFN is required and complicated mutual coupling effecte in the feed errey are evoided. The BFN end the epillover loeees are absent or drestically reduced eo that the gain delivered cen be higher. Sheped reflector antenne syetems ere in repid development end major future progress is likely with the recent edvent of rigoroue methode [60]. Work is aleo being carried out on duel reflectore [61].

6 DUAL REFLECTOR SYSTEMS WITH SMALL SCAN DEGRADATIONS

The duel offeet Cessegrain or Gregorian reflector systeme permit cancellation of the croee polerizetion for e linearly polarized on-exie beam [62]. This is echieved if the exas of the feed, the eubreflector end the main reflector are edjusted according to the condition

$$\tan \gamma/2 = 1/M \tan \psi/2 \qquad (35)$$

where γ ie the engie from the main reflector axis to the subreflector exie end ψ the engle from the subreflector exis to the feed axie (see Figure 31). The velue of the eubreflector "magnificetion" M determines the eubreflector type:

(1) $M > 1$: The subreflector is the convex brench of e hyperboloid with the eccentricity $e = (M + 1)/(M - 1)$. Thie is a conventionel duel offeet Cassegrein.

(2) $0 < M < 1$: The subreflector ie the concave brench of e hyperboloid with $e = (1 + M)/(1 - M)$. This is either the front-fed or the side-fed duel offset Ceseegrain discussed below.

(3) $M < -1$: The eubreflector is an ellipsoid with $e = (M + 1)/(M - 1)$. This is e convantional dual offeet Gregorian.

Dual offset raflactor configurationa which fulfil the condition (35) hes no first-order eetigmatism which otherwise is the dominant acan eberretion in offaet refiector antennes [30]. Conventionel compeneeted dual offset Cessagrain and Gregorian antennas, $M > 1$ and $M < -1$ above, are difficuit to design with no blockege for larga acan angles, and the faed errey is lerger than in the ceae whera the main reflector ia uaad ea single reflector. These problems are reducad when $0 < M < 1$ for tha two different configurationa in Figure 32, which both are designed for e $\pm 10^\circ$ scan. In Figura 32a, the feed array is located in front of both tha subreflactor and the main raflector and the system haa baen tarmad it the front-fad offset Cassagrein (FFOC) antenna system [63]. In the second configuretion in Figura 32b tha feed array end tha subraflector ara plecad on either sida of tha main raflactor. Thia system has been termed tha aide-fed offaat Cessagrain (SFOC) antenna syatem [53]. Both the FFOC and tha SFOC have uniqua acan propertias ovar the full $\pm 10^\circ$ fiald-of-view dua to tha larga focal length of tha main raflactor. Tha large fiald-of-view requiras thet tha subraflactor sisa ba comparabla to tha main raflactor sisa. For contiguous Earth covaraga, tha faad array sisa ia axcaasiva and tha systems may not be competitiva to an array antanna. Howavar, tha inharent property of a raflactor antanne ayetem of aasociating aingla faads with high-gain spot beams makas tha configurationa shown in Figura 32 vary attractiva candidatas for maating partial Earth covarage raquirementa with many high-gain beams.

6.1. Scan Propertiaa of tha FFOC and tha SFOC

Figuras 33 and 34 ahow tha calcuiatad principai co- and croas-polar pattarn cuta for secondary beams radiatad by small linaarly polarisad conical horna placed at tha iocations which ara corrasponda to beams on axis and with 10° downward acan, 10° upward acan and 10° latarel acan. Tha diametara of tha feeds ara 1.8 λ (FFOC) end 2.2 λ (SFOC) and corraspond to a beam apacing of 92 per cent of tha beam width. This ia cioaa to tha apacing which givaa tha highaat gain at tha cross-ovar lavei for multi-beam applicationa whara each beam is radiatad by a aingla horn. In aach casa, the feed iocation ia optimiaad to minimisa tha phesa errora and tha feed axia ia aiignad so that tha cantrai ray hita tha cantar of tha main raflactor aurfaca. For both tha FFOC and tha SFOC, tha diametar D of tha projactad apertura ia 120 λ. Tha smali feeds provida only a slight apertura tapar. This aituatior exhibita both tha highaat aidalobes and tha iargeat acan losaas. Tha calcuiatad peak diractivity, peak aidaiobe lavai and peak aidalobe iavel for tha two configurations ara given in Tabla 8. Tha peak directivity ia broken up into a number of afficianciaa

$$G_{sc} = \eta_{ap}\,\eta_{ar}\,\eta_{ap}\,G_o \qquad (36)$$

whera

- η_{ap} ia the apillovar efficiency, (tha fraction of the feed power which hits the main raflector),
- η_{ar} ia tha ralativa projected area (the ratio of the areas obtained by projacting the main raflector rim into a piana perpendicular to the direction of the acanned beam and into a plana perpendicular to tha direction of tha on-axia beam),
- η_{ap} ia tha apartura efficiency including losa due to phasa arrora, amplitude tapar and crosa polarisation. (This lose in dominated by the phasa arrors essocieted with the scan as the aperture illumination ia almost uniform), and
- G_o is the peak echievable directivity $\pi D/\lambda$ (51.53 dBi for D = 120 λ).

Beam direction	η_{sp} dB	η_{ar} dB	η_{ap} dB	Directivity dBi	Sidelobe dB	Cross-pol dB
FFOC:						
on axis	-4.62	0	-0.03	46.88	-28.38	-48.68
10° downward	-3.48	+0.75	-2.28	46.52	-3[illegible].63	-38.06
10° upward	-5.87	-1.07	-1.55	43.04	-23.14	-35.52
10° sideward	-4.78	-0.07	-0.63	46.05	-33.63	-37.40
SFOC:						
on axis	-5.09	0	-0.02	46.42	-28.01	-54.78
10° downward	-4.68	+0.34	-0.36	46.83	-33.28	-40.20
10° upward	-5.72	-0.52	-0.24	45.05	-29.88	-37.49
10° sideward	-5.29	-0.07	+0.03	46.20	-30.25	-41.56

Table 8. Peak directivity budget and peak sidelobe level of FFOC and SFOC.

Due to the relatively small feed size and small angle subtended by the subreflector rim, the feed spillover is large. The large scan causes a significant change of the relative projected area. As the main reflector is closer to vertical for the SFOC than for the FFOC, the area loss for upwards scan is smaller for the SFOC. The aperture efficiency is, except for the on-axis beam, dominated by phase errors, i.e., scan aberrations. We see that the effect of these phase errors is smaller for the SFOC. The smaller scan aberrations of the SFOC also follow from the pattern in Figures 33 and 34. The sidelobes and the cross polarization are lower for the SFOC than for the FFOC. As the aperture diameter increases, e.g., to 240λ, the superiority of the SFOC with respect to electric performance is accentuated. For both configurations, the scan losses are higher for beam scanning in the plane of symmetry than in the perpendicular plane. In the plane of symmetry, the scan losses due to phase errors are slightly higher for downward scan, but they are compensated by reduced spillover and area losses. In a practical design, the antenna axis should be repointed to equalize the overall scan loss in all directions or give preference to critical areas in the coverage. Comparisons with the single offset paraboloidal reflectors show that the FFOC achieves similar scan performance as a single offset parabola with an f/D ratio equal to about 2.6. The SFOC is comparable to a single offset parabola with an f/D of about 5.6.

More details including the initial design of a feed array to generate 10 contoured beams out of the SFOC are given in [53].

7 CONTOURED-BEAM ARRAY ANTENNAS

Table 2 indicated the significant growth of the feed array size for each new INTELSAT spacecraft series. If the trend towards larger and radiating apertures and f/D ratios continues, the feed array size will ultimately exceed the reflector size and the antenna mass and volume requirements will have a tremendous impact on spacecraft design and launch cost. Thus, it may become advantageous to "discard the reflector and turn the feed array towards the Earth" and use it as a directly radiating array.

7.1 Array Excitation Optimisation with Pencil Element Beams

We consider the planar array configuration in Figure 35. It consists of N_a elements in a hexagonal lattice. We define N_b element beams radiated by the array in a hexagonal lattice over the field-of view shown in Figure 36. The half-power beamwidth of the element beams is determined by the array diameter D and is for a uniform array illumination approximately $\Delta\theta_3 = \lambda/D$. The optimization of the array excitations to meet specified coverage and isolation requirements is carried out by the algorithms discussed in Section 3 but indirectly by optimizing the excitations of the element beams. Then, the array excitations are calculated from the element-beam excitations. The optimisation via the element beams is much more efficient than a direct optimisation of the array excitations because

(1) the number of element beam is in general much less than the number of array elements, and
(2) the element beam are almost orthogonal to each other over the far-field pattern in the sense their pattern only overlap little as opposed to the array element patterns, which overlap completely. As a result, the optimisation is a more well behaved problem.

The number of array elements for a given aperture size is determined by the requirement that no grating lobes fall in the field-of-view. The antenna designer may choose the element-beam positions independently for each coverage area of a multi-beam array antenna. This is not possible for a reflector antenna. The aperture size in wavelengths and the angular extent of the coverage area determines the number of the degrees of freedom of the synthesis problem [64]. In most cases, the beam spacing can be chosen a little larger than the beam width as in the case of a reflector antenna. No advantages are gained by choosing the beam spacing significantly smaller than the beam width.

Figure 37 shows an optimised contoured beam for an array consisting of 169 conical horns with a diameter of 2.84 λ. The array diameter is identical to the size of the INTELSAT VI hemi/zone reflector. By gradual removal of weakly excited array elements followed by re-optimisation of the remaining excitations, the number of array elements can be reduced significantly. A full account of the design procedure and many design cases have been given in [65].

8. ACKNOWLEDGEMENTS

This paper is based on work performed, in part, for the European Space Technology and Research Centre (ESTEC) of the European Space Agency and, in part, under the sponsorship and technical direction of the International Telecommunications Satellite Organization (INTELSAT). Any views expressed are not necessarily those of INTELSAT. The author wishes to thank R Jorgensen, TICRA, K Pontoppidan, TICRA, PE Frandsen, TUD, and Antoine Roederer, ESTEC. The author is grateful to former colleagues at INTELSAT in particular to DK McCarthy, W Bornemann and WJ English.

9 REFERENCES

[1] "Radio Regulations", ITU, Geneva, 1982

[2] KG Schroeder (1972), "Characteristics and applications of multi-beam spacecraft antennas", 4th AIAA Comm. Sat. Syst. Conf., Washington, D.C., paper No. 72-530

[3] P Foldes (1982), "Recent advances in multibeam antennas", 11th European Microwave Conf., Amsterdam, 59-72

[4] LJ Ricardi (1982), "Multiple beam antennas", Ch. 6 in AW Rudge, K Milne, AD Olver and P Knight (Eds.), "The Handbook of Antenna Design. Volume 1". London: Peter Peregrinus Ltd.

[5] JL Butler (1966), "Digital, matrix and intermediate-frequency scanning", Ch. 3 in RC Hansen (Ed.), "Microwave Scanning Antennas. Volume 3". New York: Academic Press, 241-268

[6] AR Dion (1982), "Lens antennae", Sect. 3.7 in AW Rudge, K Milne, AD Olver and P Knight (Eds.), "The Handbook of Antenna Design. Volume 1". London: Peter Peregrinus Ltd.

[7] HHS Luh, TM Smith and WG Scott (1982), "A dual-band TEM lens for a multiple beam antenna", IEEE Trans. Antennas Propagat., Vol. AP-30, 224-229

[8] F Taormina, DK McCarty, T Crail and D Nakatani (1976), "INTELSAT IVA communications antenna - frequency re-use through spatial isolation", Intl. Conf. on Communications, Philadelphia, 4.10-4.14

[9] CC Han, AE Smoll, HW Bilenko, CA Chuang and CA Klein (1976), "A beam-shaping multifeed offset reflector antenna", 6th AIAA/CASI Comm. Sat. Syst. Conf., Montreal, 245-249

[10] EW Matthews, CL Cuccia and MD Rubin (1979), "Technology considerations for the use of multiple beam antenna systems in communications satellites", IEEE Trans. Microwave Theory Tech., Vol. MTT-27, 998-1004

[11] MF Caulfield, FA Taormina, BM Flynn, SO Lane, TM Paige and VE Cascia (1982) "INTELSAT VI antenna system design and development", Conf. Large Space Antenna Syst. Tech., NASA Langley, 743-765

[12] SO Lane, MF Caulfield and FA Taormina (1984), "INTELSAT VI antenna system overview", 10th AIAA/CASI Comm. Sat. Syst. Conf., Orlando

[13] WJ English (1980), "Improving future communications satellite antenna designs", 8th AIAA/CASI Comm. Sat. Syst. Conf., Orlando, 464-470

[14] DF DiFonzo (1982), "Evolution of satellite antennas", IEEE Intl. Symp. Antennas Propagat., Albuquerque, 358-361

[15] P Neyrat (1984), "Antenna technology at INTELSAT", Journées Internationales de Nice sur les Antennes, Nice, pp. 69-90.

[16] WVT Rusch (1982), "Reflectors with contoured beams", Sect. 3.5 in AW Rudge, K Milne, AD Olver and P Knight, "The Handbook of Antenna Design. Volume 1". London: Peter Peregrinus Ltd.

[17] B Vidal Saint Andre and P Neyrat (1980), "The application of single reflector multi-feed antennas to direct T.V. satellites", 10th European Microwave Conf., Warszaw, 90-94

[18] A Roederer(1984), "Antennes pour satellite de télévision directe", Journées Internationales de Nice sur les Antennes, Nice, 154-167

[19] H Soule, J Rosen, J MacGahan, J Dumas and C Profera (1984), "Shaped-beam antenna for direct broadcast satellites", 10th AIAA/CASI Comm. Sat. Syst. Conf., Orlando

[20] V Galindo-Israel, Y Rahmat-Samii, W Imbriale, H Cohen and R Cagnon (1984), "A CONUS time zone DBS antenna system with single polarisation", IEEE Intl. Symp. Antennas Propagat., Boston, 143-146

[21] K Pontoppidan (1979), "Pattern prediction methods for high performance single and dual reflector antennas", Final Report S-101-02 on ESTEC Contract 3629/78/NL/AK, TICRA A/S, Copenhagen, Denmark

[22] SW Lee and Y Rahmat-Samii (1981), "Simple design formulas for designing an offset multibeam parabolic reflector", IEEE Trans. Antennas Propagat., Vol. AP-29, 472-478

[23] A Saitto (1981), "Gain-bandwidth product and other reflector antenna relationships", ESA Journal, Vol. 5, 249-258

[24] GAE Crone, A Jorgensen and AG Roederer (1984), "Comparison of contoured beam reflector antenna designs for improved European coverage", IEEE Intl. Symp. Antennas Propagat., Boston, 792-795

[25] PD Patel and KK Chan (1985), "Optimization of contoured beams for satellite antennas", Proc. IEE, Vol. 132, Pt. H, 400-406

[26] Y Rahmat-Samii and SW Lee (1983), "Directivity of planar array feeds for satellite reflector applications", IEEE Trans. Antennas Propagat., Vol. AP-31, 463-470. See also correction in Vol. AP-32, 762

[27] PJB Clarricoats, SM Tun and CG Parini (1984), "Effects of mutual coupling in conical horn arrays", Proc. IEE, Vol. 131, Pt. H, 165-171

[28] L Lewin (1975), "Expression for decoupling in multiple-beam antennas", Electr. Ltrs., Vol. 11, 420-421

[29] PJ Wood (1986), "Some extensions of the beam orthogonality concept for multi-beam antennas", IEEE Montech '86 Conf. Antennas & Comm., 310-313

[30] C Dragone (1982), "A first-order treatment of aberrations in Cassegrainian and Gregorian antennas", IEEE Trans. Antennas Propagat., Vol. AP-30, 331-339

[31] J Ruze (1965), "Lateral-feed displacement in a paraboloid", IEEE Trans. Antennas Propagat., Vol. AP-13, 660-665

[32] TS Chu and RH Turrin (1973), "Depolarisation properties of offset reflector antennas", IEEE Trans. Antennas Propagat., Vol. AP-21, 339-345

[33] NA Adatia and AW Rudge (1975), "Beam-squint in circularly polarised offset reflector antennas", Electr. Ltrs, Vol. 11, 513-515

[34] EA Ohm (1979), "Multibeam satellite antenna with optimised polarisation distribution and full U.S. coverage", IEEE Intl. Symp. Antennas Propagat., Seattle, 266-269

[35] J Jacobsen (1977), "On the cross polarisation of asymmetric reflector antennas for satellite applications", IEEE Trans. Antennas Propagat., Vol. AP-25, 276-283

[36] MJ Gans and RA Semplak (1975), "Some far field studies of an offset launcher", BELL Syst. Tech. J., Vol. 54, 1319-1340

[37] TS Bird (1982), "Contoured-beam synthesis for array reflector antennas by field correlation", Proc. IEE, Vol. 129, Pt. H, 293-298

[38] JF Bull, P Kalata and CE Profera (1982), "Application of the method of steepest descent optimization to the design of shaped beam antennas", IEEE Intl. Symp. Antennas Propagat., Albuquerque, 600-603

[39] C Dedeban, M Minoux and P Brachat (1984), "Un logiciel pour l'optimisation du diagramme de rayonnement d'une antenne à faisceau conforme", Journées Internationales de Nice sur les Antennes, Nice, 56-63

[40] S Mano, T Katagi and T Tsutsumi (1984), "Pattern synthesis of array fed reflector antennas", Electronics and Communications in Japan, vol. 67-B, No. 7, 38-45

[41] K Shamsaifar and M Calvo (1986), "Contoured beam synthesis for a small number of feeds by optimising their position and excitation", IEEE Intl. Symp. Antennas Propagat., Philadelphia, 727-730

[42] RFE Guy (1985), "A synthesis technique for array antennas of general shape with various aperture constraints", 4. Intl. Conf. Antennas Propagat., Warwick, 35-39

[43] GT Poulton (1986), "Antenna power pattern synthesis using method of successive projections", Electr. Ltrs., Vol. 22, 1042-1043

[44] AI Zaghloul and DK Freeman (1986), "Phased array synthesis for shaped beams using power matrix method", IEEE Intl. Symp. Antennas Propagat., Philadelphia, 177-180

[45] D Kawabata, M Uano, T Morroke, T Chiba, R Kawashima, W Bornemann and WJ English (1986), "Synthesis of spacecraft antennas by use of Fourier transform method", IEEE Intl. Symp. Antennas Propagat., Philadelphia, 719-722

[46] JR Maute and RF Harrington (1975), "Computational methods for antenna pattern synthesis", IEEE Trans. Antennas Propagat., Vol. AP-23, 507-512

[47] K Madsen (1975), "Minimax solution of non-linear equations without calculating derivatives," Math. Prog. Study, Vol. 3, 110-126

[48] CG Broyden (1965), "A class of methods for solving non-linear simultaneous equations", Mat. of Comp., Vol. 19, 577

[49] K Madsen and H Schaer-Jacobsen (1976), "Singularities in minimax optimization of networks", IEEE Trans. Circuits and Systems, Vol. CAS-23, 456-460

[50] CA Klein (1984), "Design of shaped-beam antennas through minimax gain optimisation", IEEE Trans. Antennas Propagat., Vol. AP-32, 963-968

[51] L Deemen (1986), "Etude d'optimisation d'antennes multisources", M.Sc.EE Thesis, Faculté des Sciences Appliquées, Université de Liège

[52] P Foldes, F Rispoli and R Jorgensen (1986), "Antenna design for the Eutelsat program", IEEE Intl. Symp. Antennas Propagat., Philadelphia, 165-168

[53] R Jorgensen, P Balling and WJ English (1985), "Dual offset reflector multi-beam antenna for international communications satellite applications", IEEE Trans. Antennas Propag., Vol. AP-33, 1304-1312.

[54] S Adatia, P Balling, B Claydon, P Ingvarson and A Roederer (1980), "A European contoured beam reflector antenna development", 10th European Microwave Conf., Warsaw, 95-99

[55] DJ Brain, A Brunt, WT Costello, Y Kol, MS Sidat and R Waugh (1985), "A circularly-polarised antenna for contoured beam coverage of Europe", 4th Intl. Conf. Antennas Propagat., Norwich, 536-540

[56] T Katagi and Y Takeichi (1975), "Shaped-beam horn reflector antenna", IEEE Trans. Antennas Propagat., Vol. AP-23, 756-763

[57] H Kumazawa, T Katagi and T Ebisui (1983), "Shaped-beam horn reflector antennas with aperture phase distribution modified by a plane wave", IEEE Intl. Symp. Antennas Propagat., Houston, 338-341

[58] R Jorgensen (1980), "Coverage shaping of contoured-beam antennas by aperture field synthesis", Proc. IEE, Vol. 127, Pt. H, 201-208

[59] B Cornblaat (1976), "Microwave Optics". London: Academic Press, 380-383

[60] BS Westcott (1983), "Shaped Reflector Antenna Design". Letchworth, Hertfordshire, England: Research Studies Press Ltd.

[61] N Adatia and S Tun (1986), "Shaped dual offset reflector antennas for contoured beam spacecraft applications", Journées Internationales de Nice sur les Antennes, Nice, 148-153

[62] H Tanaka and M Mizusawa (1975), "Elimination of cross-polarisation in offset dual-reflector antennas", Electronics and Communications in Japan, Vol. 58-B, No. 12, 71-78

[63] S Makino, Y Kobayashi, B Urasaki and T Katagi (1984), "Front fed offset Cassegrain type multibeam antenna", National Convention of IECEJ

[64] JT Mayhan (1976), "Nulling limitations for a multiple beam antenna", IEEE Trans. Antennas, Propagat., Vol. AP-24, 769-779

[65] W Bornemann, P Balling and WJ English (1985), "Synthesis of spacecraft array antennas for Intelsat frequency reuse multiple contoured beams", IEEE Trans. Antennas Propagat., Vol. AP-33, 1186-1193

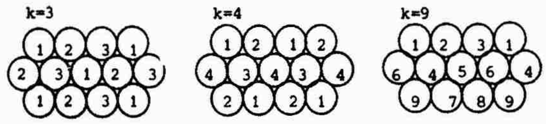

Figure 1 Multi-beam beam topologies for frequency re-use.

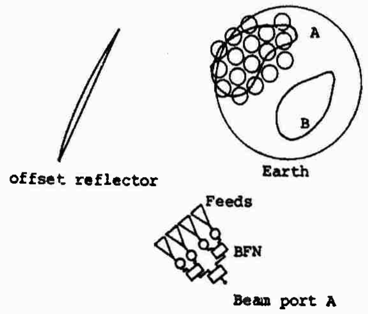

Figure 2 Contoured beam from offset reflector with feed array and BFN

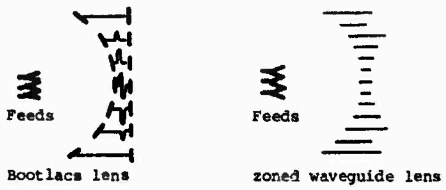

Figure 3 Microwave multi-beam lens antennas

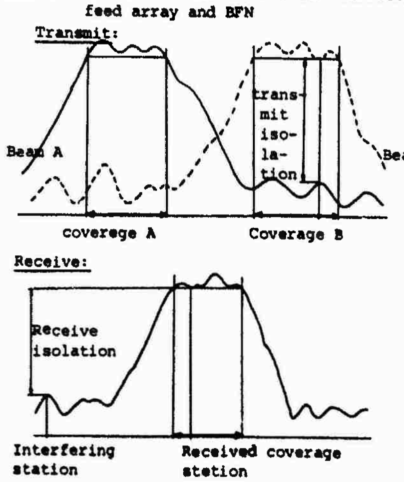

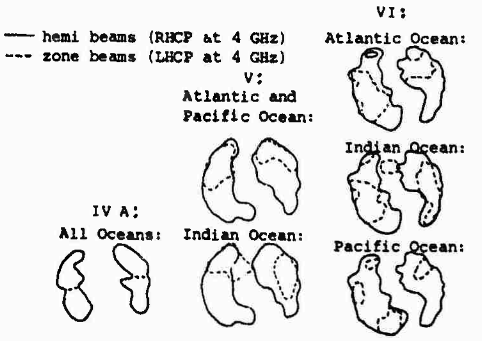

Figure 5 Growth in the complexity of the INTELSAT spacecraft hemi/zone coverages

Figure 4 Definition of isolation for transmit and receive contoured-beam antennas.

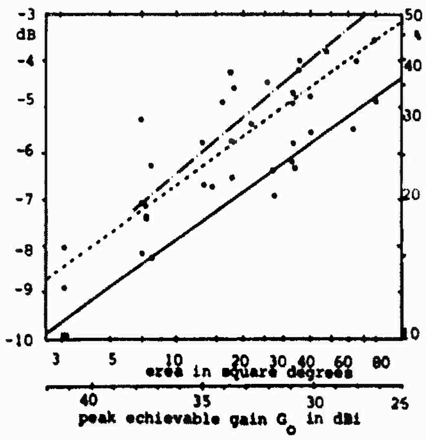

Figure 6 Contoured-beam efficiencies versus coverage area size for 3.2 m reflector at 4 GHz. The lines are determined by linear regression for the following three cases:
—— INTELSAT VI antenna (oo)
---- similar but with 1.3λ feeds (oo)
-.-. similar but with 1.3 feeds and relaxed coverage area specs. (oo)

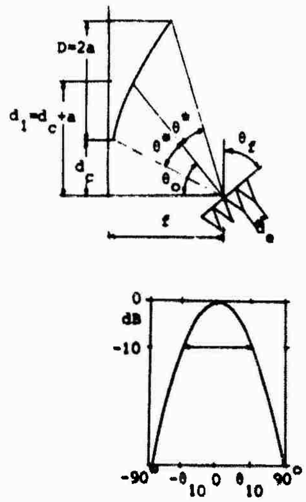

Figure 7 Reflector and feed parameters used in the simple analytic beam model.

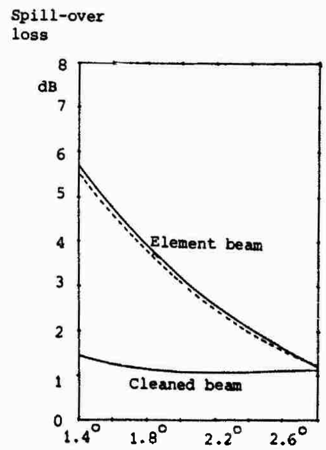

Figure 8 Spillover loss vs. spacing of component beams.
—— simple analytic beam model
---- reflector antenna analysis program

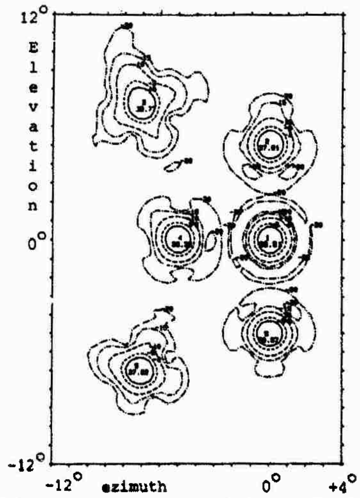

Figure 9 Gain contours 1, 3, 5, 10, 15 and 20 dB below peak gain level for on-axis and scanned element beams in a 43λ diameter offset-fed paraboloid.

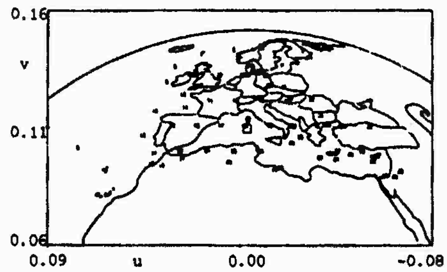

Figure 10 Examples of discrete stations (or sampling points) representing coverage-area specifications.

Figure 11 Contour plots for best analytical beam configuration →

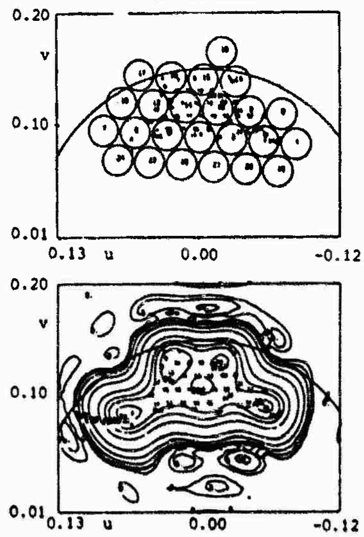

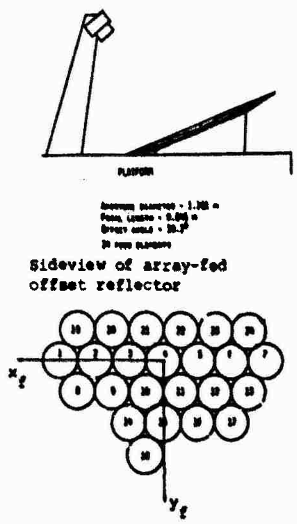

Figure 12 Initial ECS contoured beam reflector and feed array

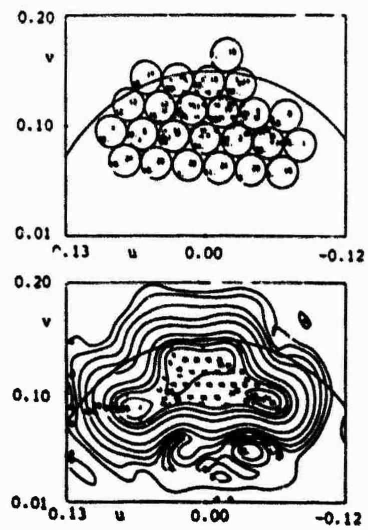

Figure 13 PO/GTD element beams and contoured beam at 10.7 GHz →

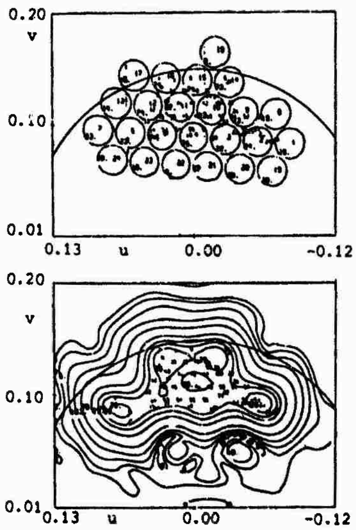

Figure 14 PO/GTD element beams and contoured beam at 11.7 GHz

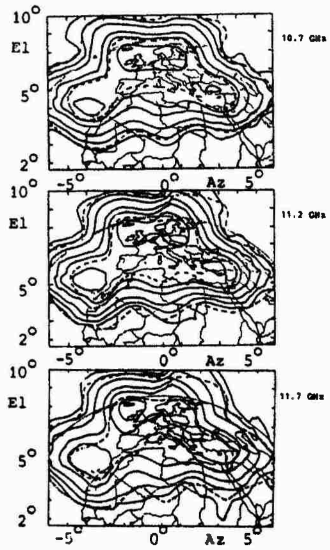

Figure 15 Measured gain contours 1, 3, 5, 10, 15 and 20 dB and calculated gain contours 3 and 20 dB below peak gain for ECS coverage array-fed contoured-beam reflector antenna

—— measurements (ERA)

----- calculation

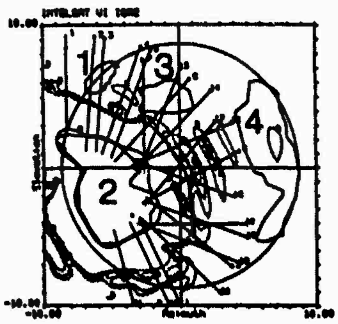

Figure 16
Nominal I-6 IOR zone 2 contours

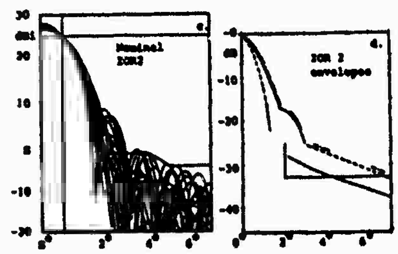

Figure 17 Gain roll-off patterns traces and envelopes ofr I-6 IOR zone 2.

Figure 18
IOR 2 synthesis stations

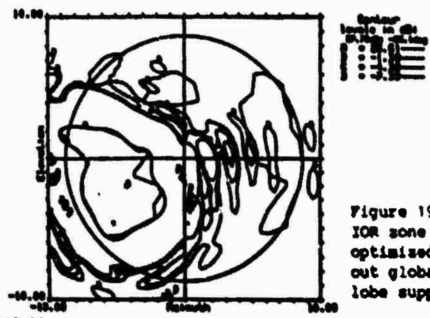

Figure 19
IOR zone 2 beam optimized without global sidelobe suppression

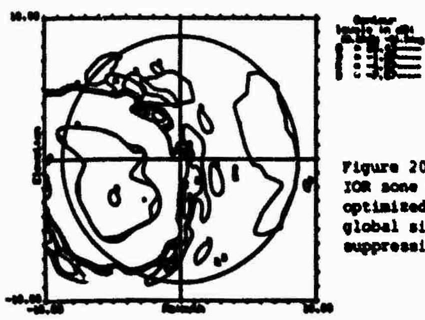

Figure 20
IOR zone 2 beam optimized with global sidelobe suppression

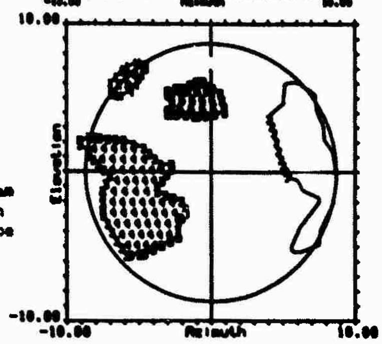

Figure 21
Synthesis stations for Indian Ocean region zone 2 beam

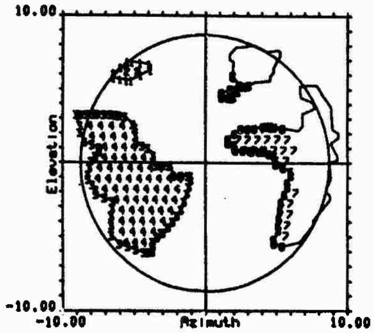

Figure 22 Synthesis stations for Atlantic Ocean region zone 2 beam

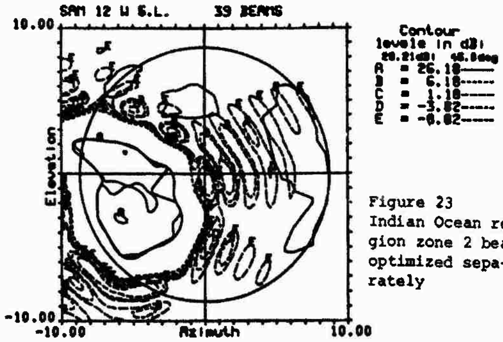

Figure 23 Indian Ocean region zone 2 beams optimized separately

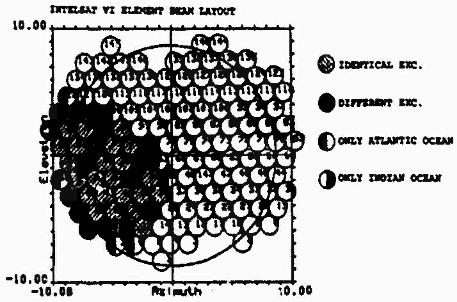

Figure 25 Shared and separate excitations for Indian and Atlantic Ocean region 2 beams

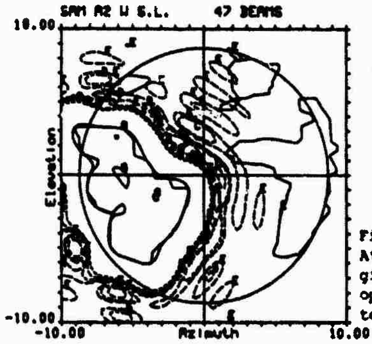

Figure 24 Atlantic Ocean region zone 2 beams optimized separately

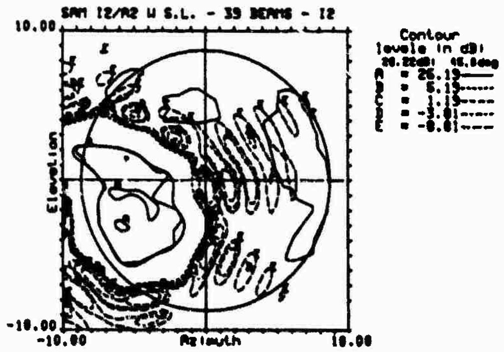

Figure 26 Indian Ocean region zone 2 beam optimized with 23 feeds common with Atlantic Ocean region zone beam

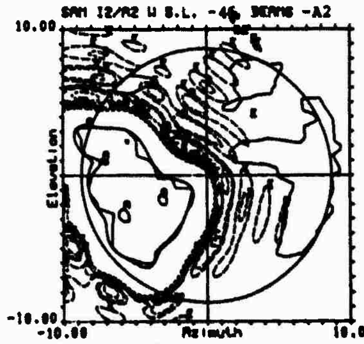

Figure 27 Atlantic Ocean region zone 2 beam optimized with 23 feeds common with Indian Ocean region zone beam

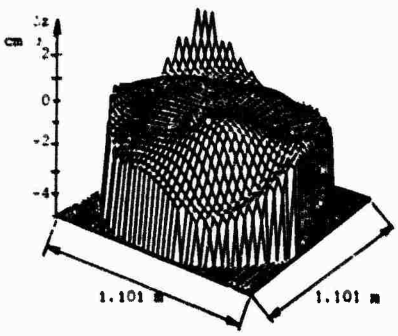

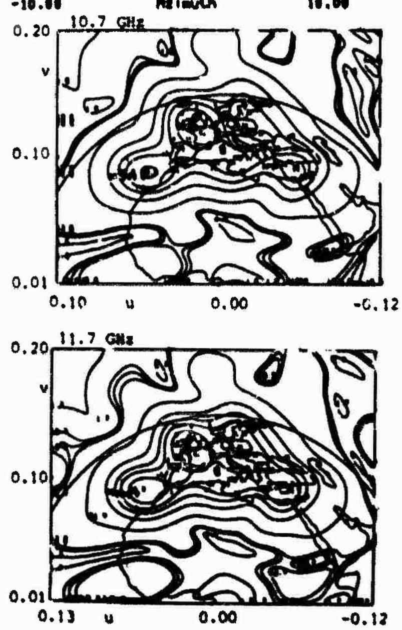

Figure 28 Deviations Δz of shaped reflector surface from paraboloid.

Figure 29 Isodirectivity curves for shaped reflector at edges of frequency band.

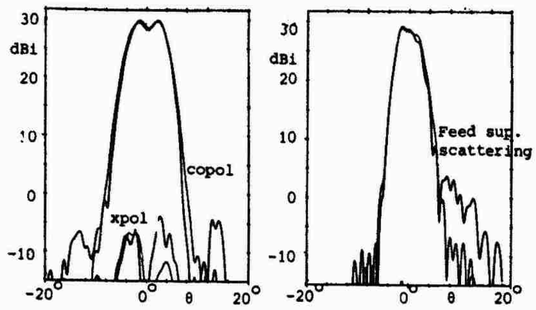

Figure 30 Measured and calculated principal pattern cuts at 11.7 GHz for shaped contoured-beam reflector.
——— measurement (TUD)
----- calculation

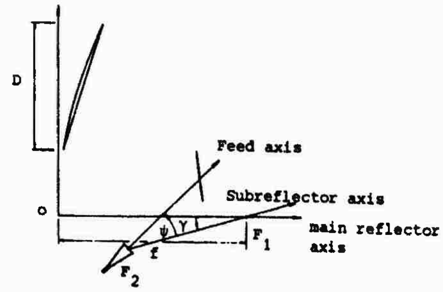

Figure 31 Conventional dual offset Cassegrain compensated for cross polarization and astigmatism

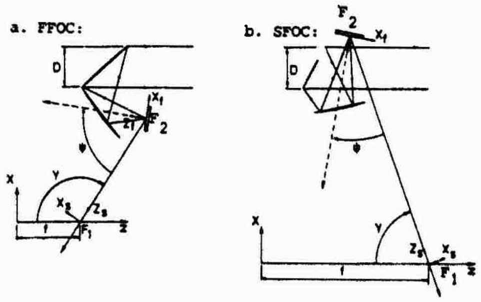

Figure 32 Alternative dual offset Cassegrain antennas compensated for cross polarization and astigmatism

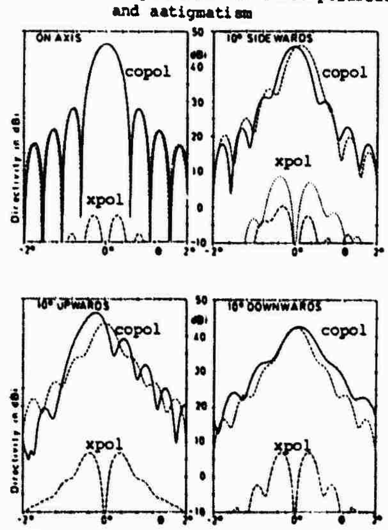

Figure 33 Principal pattern cuts for element beams in 120λ FFOC.

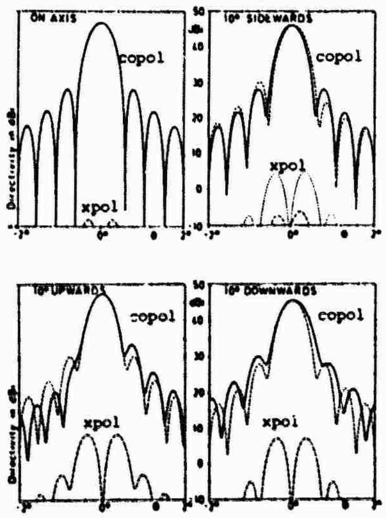

Figure 34 Principal pattern cuts for element beams for 120λ SFOC.

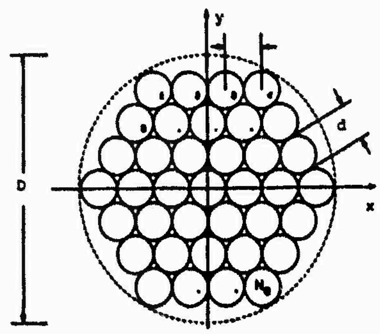

Figure 35 Array antenna element configuration

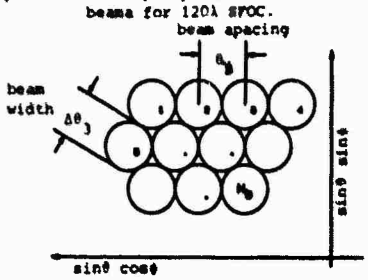

Figure 36 Array antenna element beams

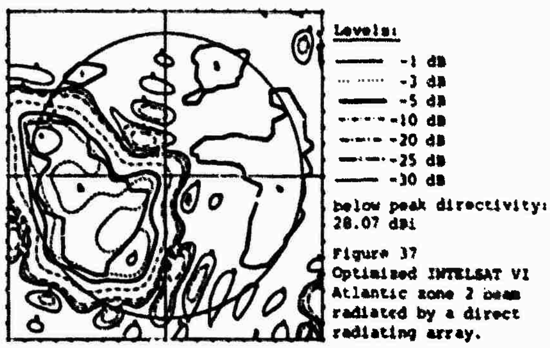

Figure 37
Optimized INTELSAT VI Atlantic zone 2 beam radiated by a direct radiating array.